Smoke-Column Observations from Two Forest Fires Using Doppler Lidar and Doppler Radar

R. M. BANTA, L. D. OLIVIER, E. T. HOLLOWAY, R. A. KROPFLI,
B. W. BARTRAM, R. E. CUPP, AND M. J. POST

NOAA/ERL Wave Propagation Laboratory, Boulder, Colorado

(Manuscript received 28 August 1991, in final form 2 March 1992)

ABSTRACT

To demonstrate the usefulness of active remote-sensing systems in observing forest fire plume behavior, we studied two fires, one using a 3.2-cm-wavelength Doppler radar, and one more extensively, using Doppler lidar. Both instruments observed the kinematics of the convection column, including the presence of two different types of rotation in the columns, and monitored the behavior of the smoke plume.

The first fire, a forest fire that burned out of control, was observed by the Doppler radar during late-morning and afternoon hours. Strong horizontal ambient winds produced a bent-over convection column, which the radar observed to have strong horizontal flow at its edges and weaker flow along the centerline of the plume. This velocity pattern implies that the column consisted of a pair of counterrotating horizontal vortices (rolls), with rising motion along the centerline and sinking along the edges. The radar tracked the smoke plume for over 30 km. It also provided circular depolarization ratio measurements, which gave information that the scattering particles were mostly flat or needle shaped as viewed by the radar, perhaps pine needles or possibly flat ash platelets being viewed edge on.

The second fire, observed over a 5-h period by Doppler lidar, was a prescribed forest fire ignited in the afternoon. During the first hour of the fire the lidar observed many kinematic quantities of the convection column, including flow convergence and anticyclonic whole-column rotation of the nearly vertical column, with a vorticity of approximately 10^{-2} s^{-1} and an estimated peak vertical velocity w of 15 m s^{-1}. After the first hour ambient meteorological conditions changed, the whole-column rotation ceased, and the convection column and smoke plume bent over toward the lidar in stronger horizontal flow. At two times during this later stage, w was estimated to be 24 and 10 m s^{-1}. Lidar observations show that the smoke plume of this second fire initially went straight up in the convection column to heights of over 2 km, so most of the smoke was injected into the atmosphere above the unstable, afternoon, convective boundary layer, or mixed layer. Later, as the horizontal winds increased, a larger fraction of the smoke remained in the mixed layer. Finally, very late in the afternoon, after ignitions had ceased and the fire was smoldering, almost all of the smoke remained within the mixed layer.

These analyses show that lidar and radar can provide valuable three-dimensional datasets on kinematic quantities and smoke distribution in the vicinity of fires. This kind of information should be of great value in understanding and modeling convection-column dynamics and smoke-plume behavior.

1. Introduction

Wildland fires are generally wind-driven surface phenomena. Occasionally fires grow upward from two-dimensional (horizontal) surface fires of reasonably predictable behavior into three-dimensional fires, in which the fire itself generates the winds that drive the fire. In wildland firefighting, this is called a "blowup" condition, and the spread of the fire as well as the fire behavior are far less predictable. Models—conceptual, theoretical, and numerical—of the interaction of the fire with the atmosphere above the fire are needed to predict the behavior of the surface fire and the convection column. High-quality observations of the internal structure and the external environment of fires and convection columns are vital to the development of useful models.

The models must be complex because fires and the atmosphere interact strongly. Fires affect the atmosphere by disturbing the ambient airflow and injecting smoke, heat, and other emittants above the surface of the earth. Atmospheric conditions affect fires, since atmospheric wind, moisture, and temperature influence fuel dryness, control fire behavior, determine rates of spread, and distribute windborne flaming debris (firebrands) ahead of the fire.

Predicting fire behavior is of great interest because lives and property are often at stake. Nationally, more people are choosing to live in areas with large accumulations of forest biomass, that is, in the so-called urban–wildland interface region, and risks to people as well as firefighters attempting to protect the lives and property are great. The ability to predict fire be-

---

Corresponding author address: Dr. Robert M. Banta, NOAA/ERL: R/E/WP2, 325 Broadway, Boulder, CO 80303-3328.

havior is also important because of the increased use of prescribed burning in recent decades to help prepare logged areas for replanting. Lives have been lost during prescribed burns, when the fires defied predictions and burned out of control. For these reasons it is highly desirable not only to understand but also to be able to predict fire behavior.

In this study we address two questions on the interaction between fires and the atmosphere: 1) Where does the smoke plume go, and what are its characteristics? and 2) What are properties of the flow inside and immediately around the convection column? The second question is a significant part of the larger question: How does fire behavior depend on external conditions? In this study internal convection-column behavior has been observed using two active remote-sensing systems, a Doppler radar and a Doppler lidar. This is the first time that pulsed Doppler lidar has been used to study a forest fire.

Answering the first question is of interest on both local and global scales. On local scales knowing the impact of smoke on populated areas downwind of fires is a key aspect of prescribed-burn policy and decision making. On global scales many gaseous emittants that accompany smoke are active as greenhouse gases and therefore may affect climate. Climate-change implications of micrometer-sized smoke particles themselves that would result from huge numbers of large fires ignited by a nuclear war have been investigated as a part of the "nuclear winter" controversy (e.g., Pittock et al. 1986). Although research has indicated that such devastating global results are not likely, reminders exist in the historical fire literature (Lyman 1918; Wexler 1950; Smith 1950; Shostakovitch 1925) of continental-scale smoke palls from extensive forest fires in North America and Siberia. The smoke palls obscured the sky and caused cool summertime surface temperatures in regions downwind. Thus, extensive smoke plumes can have synoptic- and climatological-scale impacts that are not so dramatic as nuclear winter but that are still significant. Observations of smoke, including, for example, the heights that smoke emissions achieve and whether the smoke passes through a capping cumulus cloud, thus address a range of issues over a broad range of scales.

Answering the second question is essential to understanding and predicting the behavior of large fires. Improving predictions of fire behavior requires careful observational studies of the relationship between ambient atmospheric conditions and fire behavior. The atmosphere outside a fire can be adequately documented at a distance using conventional, in situ instrumentation, such as instrumented balloons, towers, and aircraft. Within the convection column, however, data on the behavior and characteristics of the fire and the column are accessible to such instrument systems only after extensive design modifications have been implemented, such as the water-cooled anemometry system described by Palmer and Northcutt (1972). Observations, such as peak vertical velocities and other kinematic quantities in the convection column, often need to be taken in the hostile environment of the column itself. For these measurements remote-sensing techniques offer the safest, often the most cost-effective, and sometimes the *only* means for obtaining the needed data.

Two issues related to the second question that can be studied using remote sensing data are whether fires are wind driven or buoyancy dominated, and whether rotation is present in a convection column. These issues are discussed in section 2. A third issue discussed in section 2 is the role of remote-sensing observations in developing numerical modeling tools for studying fire behavior.

Two fires that burned during the summer of 1988 were studied by the Wave Propagation Laboratory (WPL) of the National Oceanic and Atmospheric Administration (NOAA) Environmental Research Laboratories (ERL) to ascertain the usefulness of active remote-sensing instruments in determining fire structure and behavior, and to address these questions. WPL's Doppler radar obtained data during a wildfire in September in the foothills of the Rocky Mountains in central Colorado, and the Doppler lidar investigated a prescribed burn in northern Ontario, Canada, during August.

A fire that eventually consumed 1280 ha (3165 acres) burned out of control in Left Hand Canyon, 12 km west-northwest of Boulder, Colorado, from 7 to 13 September 1988. It was observed on 10 September 1988 with a 3.2-cm-wavelength (X-band) Doppler radar operated by WPL. The day was very windy, with surface winds gusting to more than 20 m s^{-1}. These ambient low-level winds produced a very active fire with an extensive smoke plume that proved to be an excellent subject for the radar.

During the 700-ha prescribed burn in Battersby Township in northern Ontario, on 12 August 1988, the Doppler lidar system probed the smoke-plume and velocity structure of the convection column of the fire and its environment. It scanned from a location about 6.5 km northeast of the center of the burn area, and therefore, with the southwesterly winds that blew for much of the afternoon, the lidar was downwind of the fire. The lidar monitored the vicinity of the burn site for approximately 5 h, from about 1 h before the first ignition, which occurred a little after 1300 local standard time (LST) or 1700 UTC, to about 1 h after the end of ignition, or until approximately 1800 LST (2200 UTC).

Section 3 contains descriptions of the radar and lidar instruments used in this study and descriptions of the locations of the observations. The lidar system is described at some length, because it is not a familiar meteorological instrument. The radar results are given in section 4, and the lidar results in section 5. The emphasis in this study is on the lidar observations of the Canadian prescribed burn, because that fire was studied more systematically from start to end. Section 6 contains a summary of the findings and a discussion of the implications of these findings to the issues raised in sections 1 and 2.

2. Background

a. Wind-driven versus buoyancy-dominated convection columns

Forest and wildfires are most often surface phenomena driven by the wind. The behavior and spread rate of such fires are reasonably predictable (at least to the extent that the winds themselves and other atmospheric variables, such as stability and humidity, are predictable). When winds in the lower 2–3 km of the atmosphere are light, however, the buoyancy of the hot gases in the convection column can produce strong vertical growth of the column, and therefore the fire is no longer a two-dimensional, surface phenomenon. These strong updrafts and subsequent downdrafts in turn can drive strong horizontal inflows and outflows near the surface, which spread the fire independently of the ambient winds. This condition is dangerous for two reasons (Rothermel 1991): 1) Indrafts and turbulence created by the deep circulations feed fresh air to the fire, allowing it rapidly to intensify. These fires can be very dangerous, and their behavior and spread are far less predictable than for wind-driven fires. 2) Usually such vertical development produces cumulus clouds atop the convection columns. If the atmosphere is also favorable for *deep* moist convection (cumulus congestus or cumulonimbus), the danger of strong evaporative downdrafts or "downbursts" from these clouds is high. According to Rothermel, "these winds can be extremely strong, . . . and can greatly accelerate a fire," and they are highly unpredictable.

A useful criterion for determining when fire dynamics are apt to be driven by fire-generated buoyancy is the ratio of kinetic-energy (KE) generation by the buoyancy to the rate of KE supply by the ambient wind flow (Byram 1959). When buoyancy generation is less than the rate of supply of horizontal KE by the ambient flow, the fires are wind driven. When the buoyancy generation equals or exceeds the supply of KE by the ambient flow, however, the potential for dangerous blowup fires exists. Fires with such buoyancy-dominated dynamics have been called "plume-dominated" fires by Rothermel (1991). Aronovitch (1989) has recently applied this criterion to several fires for which data were available.

In the present study the Colorado fire observed by the radar was strongly wind driven. The convection column of the Ontario fire observed by the lidar started out as buoyancy dominated, but became more wind driven throughout the period of observation.

b. Rotation in the convection column

An important kinematic quantity that can often be measured by remote sensing is rotation in the convection column. The presence of rotation in an ascending atmospheric column, such as the convection column of a fire, may significantly affect the dynamics of such a column.

The effects of rotation on another type of atmospheric structure with a strong updraft, the thunderstorm, has received considerable attention. For example, Lilly (1986) discussed effects of rotation, or "helicity," on severe thunderstorms. Helicity, the dot product of the velocity and vorticity vectors, is often high in a rotating updraft because the velocity and vorticity vectors are nearly parallel. Lilly (1986) cited several studies that show that "the effect of helicity is to reduce the diffusing and dissipating effects of turbulence upon rotating storms" and other atmospheric systems. Rotation is thus hypothesized to allow the column to achieve greater updraft strength and to penetrate to greater heights than a nonrotating column would. In the case of a fire, the increased updraft vigor could create stronger surface flow converging into the fire, increasing the oxygen supply and invigorating the fire.

The studies cited by Lilly (1986) relating helicity to the suppression of turbulent dissipation were laboratory and numerical studies, so their application to the atmosphere, and to convection columns of large fires, is largely suggestive. However, observations of large numbers of convection columns by McRae and Flannigan (1990), Graham (1955), and Church et al. (1980) support the hypothesis that rotation contributes to fire intensity. They found that the most intense columns over fires are vertical columns exhibiting whole-column rotation.

Fires exhibit many types of rotation. McRae and Flannigan (1990) identified two types of fire whirlwind that have a similar width scale to the radius of the convection column: type I vortices, which form downwind of the column, and type II vortices, in which the entire column stands nearly vertically and rotates. This classification ignores fire whirlwinds and swirls that are much smaller than the radius of the convection column. In other literature Church et al. (1980) referred to horizontal counterrotating vortices (described in the next paragraph) as "type 1" vortices and vertical, whole-column rotation as "type 3" vortices. Haines and Smith (1987) discussed examples of the former type of plume, which they called a "horizontal vortex pair."

Included with McRae and Flannigan's (1990) type I vortices are those that occur as bent-over columns in moderate to strong ambient winds. Usually these plumes consist of a pair of counterrotating horizontal vortices, or "rolls," on either side of the plume centerline, with rising motion along the centerline and sinking motion along the edges of the plume. Because this type of plume produces two distinct vortices, it is sometimes referred to as a "bifurcating" plume. According to Church et al. (1980), it occurs most often in moderate ambient flow of 4–8 m s^{-1}.

Rotation of the entire vertical column (type II) is less common than other kinds, but it can produce the most intense vortices. Whirlwinds of near-tornadic intensity have been reported in forest fires (e.g., Graham 1955) and in prescribed burns (e.g., McRae and Flannigan 1990). The most likely mechanism for producing whole-column rotation is the convergence of preexisting environmental vorticity into the convection column, according to Church et al. (1980). Other candidate mechanisms include the tilting into the vertical of the vorticity in the vertical shear of the horizontal winds near the surface. Conditions that favor the formation of type II vortices by the concentration of environmental vorticity include light (<3 m s^{-1}) boundary-layer winds, a very intense fire, an unstable lapse rate in the atmospheric surface layer, the presence of vertical vorticity in the environmental wind field, and "the development of sufficient low-level convergence to concentrate the weak background vertical vorticity," (Church et al., p. 693), that is, the development of strong upward velocities above the fire (Church et al. 1980; McRae and Flannigan 1990). If the tilting of shear vorticity is an important mechanism in developing whole-column rotation, then sufficiently strong horizontal shear vorticity and a mechanism (presumably flow into the updraft) for tilting the vorticity into the vertical must be considered as favorable conditions.

Other external factors also affect the development of rotation in a convection column. Graham (1955) found topographical influences on the generation of vortices: "Fire whirlwinds seem to develop more readily on lee slopes close to ridge tops." McRae and Flannigan (1990) found that ignition patterns of prescribed burns affect rotation in the column. "Strip-head fires," or fires that are ignited in crosswind lines, seem to favor vortex development, whereas center-fire ignitions seem to suppress column rotation.

Because of the hypothesized significance of rotation to the dynamics of a convection column it is important to be able to observe whether rotation is present, to determine what kind of rotation is occurring, and to measure quantities that characterize column dynamics, such as velocity differences, rotation rates, or vorticities. In the present study we use lidar and radar to study the rotation characteristics of two different kinds of convection column.

c. Role of numerical modeling

There are many kinds of models, including conceptual, theoretical, and numerical. Predictions and forecasts of the behavior of a fire based on current atmospheric conditions are implicitly based on conceptual models. Insight into basic physics is the aim of theoretical models, and often such models are so simple that they are not useful for real-life prediction. Numerical models, especially sophisticated three-dimensional dynamic models, attempt to solve the full nonlinear set of equations for momentum, energy, and substance continuity on a grid. Thus, they are capable of describing many of the complex interactions between a fire and the atmosphere.

Numerical models can have an important role in understanding the relationship between the characteristics of a fire and its environment. The behavior of the convection column above a large fire depends upon a great many external parameters, such as the energy-release rate (heat input) of the fire near the surface, the ambient winds and turbulence, ambient humidity, atmospheric stability, the nature of the terrain, and perhaps other more elusive effects, such as the ambient low-level vorticity in the vicinity of the fire or, in the case of a prescribed burn, the pattern of ignition of the fire. Model sensitivity studies can show to which of these parameters fire behavior is strongly sensitive and to which it is less sensitive. For example, the significance of rotation to the dynamics of a buoyant plume was discussed in section 2b. A possible feedback between rotation and intensity of the convection column of a fire was hypothesized. If such a positive feedback occurs in fires in nature, it would be of great interest to study numerically the sensitivity of rotating fire columns to varying external conditions, such as environmental vorticity or low-level vertical shear of the wind.

Three-dimensional numerical, cloud-scale dynamic models have been used to study the relationship between fire behavior and external conditions. Cotton (1985) performed such calculations using a three-dimensional cloud model, and other researchers made further experiments with the model used in Cotton's study (see Pittock et al. 1986, pp. 110–115). These simulations, along with similar results reported by Penner et al. (1986), showed that the height of penetration of the smoke column depends strongly on the energy released by the fire and on the moisture and stability in the ambient atmosphere; more intense fires, higher moisture contents, and weaker stabilities favor deeper vertical penetration. In particular, smoke columns in these models do not penetrate above the middle troposphere [4–5 km above ground level, (AGL)] without latent heat release and deep moist convection. These models do not carry oxygen as a variable and thus do not calculate the oxygen deficiency in the combustion zone, which is probably responsible for the pulsating, time-dependent nature of real fires (Palmer et al. 1991).

These model runs also did not simulate actual fires. Thus, a critical role for observational studies of fires is to provide comprehensive, high-resolution datasets of actual fires, by which dynamic numerical cloud-scale models can be initialized and verified. Recently Molencamp and Bradley (1991) reported on impressive three-dimensional simulations based on data from two fires, the Battersby Township burn described here and a Canadian prescribed burn in Hardiman Township, Ontario, during the summer of 1987.

3. Lidar and radar characteristics and locations

a. Radar

In the Colorado study, the WPL 3.2-cm-wavelength Doppler radar was located at the Boulder Atmospheric Observatory (BAO) about 28 km east-southeast of the source of the main plume from the Left Hand Canyon fire and 500 m below the level of the fire. It was used to measure Doppler velocity, reflectivity, and circular depolarization ratio (CDR). The spatial resolution of about 100 m and the accuracy of velocity measurements, about 0.5 m s^{-1}, proved to be suitable for making detailed observations of smoke plumes with radar. A Doppler radar was previously used successfully to measure turbulent velocity fluctuations within the smoke plume during Project Flambeau (Lhermitte 1969; Palmer 1981).

Scanning procedures used in these observations consisted of low-elevation sector scans to document the structure of the fire and high-elevation conical scans through 360° in azimuth to measure wind profiles using velocity–azimuth-display (VAD) techniques, as discussed in section 3b. The resulting gray-shade depictions of the data as shown in Fig. 4 are direct displays of the data and are not subjected to any smoothing other than the smoothing associated with the radar pulse volume. No transformation from spherical to Cartesian coordinates is performed. Operating characteristics of this radar are given in Table 1.

The radar transmits radiation that is circularly polarized in one sense, that is, either left-hand circular-polarized (LH) or right-hand circular-polarized (RH) radiation. The radar receiver has two separate channels, one for detecting the RH portion of the signal and one for the LH portion. Backscattering by spherical targets such as cloud or rain droplets reverses the direction of propagation of the radiation and thus reverses the sense of the polarization from LH to RH. In an example where a radar transmits LH radiation, therefore, *all* returning radiation from spherical (nondepolarizing) targets will be received in the RH or main channel and none in the cross channel. The depolarization ratio, or the ratio of power returned in the cross channel to power returned in the main channel, is thus zero, and the CDR (in decibels) is $-\infty$. In practice the received power in the cross channel is never exactly zero, because of nonideal characteristics of the antenna and microwave components. For the radar used in this study, CDR measured from nondepolarizing scatterers is -27 dB.

TABLE 1. Operating characteristics of the NOAA/WPL X-band Doppler radar

Quantity	Value
Frequency	9.3 GHz
Peak power	40 kW
Range resolution	112 m
Beamwidth	0.8°
Minimum reflectivity at 10 km	−18 dBZ
Minimum measurable CDR	−27 dB

Scatterers viewed by the radar as nonspherical do depolarize the signal: the greater the eccentricity, the greater the depolarization. The extreme case is that of linear or needlelike targets, which scatter equal amounts of RH and LH radiation back to the radar, regardless of the orientation of the scatterers. The ratio of power received in the cross channel to that in the main channel is about 1, and thus, for such targets the CDR equals 0 dB. Such values have been observed to be characteristic of dipole scatterers such as radar chaff (Moninger and Kropfli 1987). Therefore, CDR measurements give useful information on the shape of the scatterers.

b. Lidar

A lidar is a remote-sensing instrument similar to a radar, except that lidar transmits a pulse of light instead of radio-frequency waves. The lidar in the present study was developed by WPL. The light transmitted by this lidar is eye-safe infrared (IR) with a wavelength of about 10.6 μm. The transmitted beam is scattered by atmospheric aerosols (in this case mainly smoke particles or cloud droplets), and a small fraction of the scattered energy is then received back at the instrument. From this returned signal two kinds of information are processed by the lidar's computers: backscattered intensity, which is related to the size, shape, concentration, and refractive index of the scatterers, and the Doppler-shifted frequency of the returned signal, which provides an estimate of the radial component of the wind speed from the location of the lidar. Throughout this paper, "radial wind" u_r will refer to this lidar-centered (or radar-centered) radial component of the wind, and not to the component of flow converging into the convection column of the fire.

Our signal-processing equipment gives these two kinds of information (backscatter signal and u_r) averaged over discrete range intervals of 300 m, from a minimum range of 1.5 km to a maximum range of up to 30 km, depending on atmospheric attenuation conditions. Both high absolute humidities and low atmospheric aerosol concentrations (i.e., a clean atmosphere) restrict the lidar's range. Dewpoints were very high during the first hour or so of the Battersby burn (greater than 22°C), and therefore the maximum range was only about 7 km; however, later, as the atmospheric boundary layer dried out and became dirtier from the smoke, the range grew to greater than 15 km. Because the lidar beam is strongly attenuated by water droplets, clouds with significant liquid water content are essentially opaque to the lidar. In the present data this characteristic showed up as a dropout of the signal when cumulus clouds intercepted the beam. Backscatter data presented here were corrected for range and water vapor attenuation. Water vapor corrections used the nearest hourly radiosonde sounding taken by the University of Washington at the lidar site (Radke and Locatelli 1988).

Further details on the characteristics of the lidar were given by Post et al. (1981), Hardesty et al. (1983), Hardesty et al. (1987), and Post and Cupp (1990). A brief history of the development and major applications is given by Hall et al. (1987), and Hall et al. (1984) present an evaluation of the accuracy of lidar wind profiles using the VAD technique.

1) BACKSCATTER

For some interpretations of the analyses of lidar data we must know which sizes of smoke and other aerosol particles contribute most to the strong lidar returns that mark the plume. In normal, clear-air situations the strongest backscatter returns to the lidar come from scattering by particles of about 2-μm diameter (Post 1978). An example of the kind of aerosol-size distribution that produces such returns is the background aerosol distribution shown in Fig. 1a, obtained by the University of Washington's Convair aircraft sampling system during the Battersby Township burn. Inside the smoke plume (Fig. 1b) the number density of all sizes of particles increases by at least a factor of 10^2, but 1) the number of small particles with diameters of about 0.2 μm dramatically increases and 2) larger particles in the smoke with diameters of 5–40 μm either did not appear in the background samples or were below the detection threshold of the sampling system. This in-plume distribution is typical of other such distributions, such as the three presented by Radke and Ward (1991) and Radke et al. (1991). It especially resembles their Myrtle fire data, which contain a significant number of particles in the "coarse-particle mode" (greater than 2-μm diameter), as seems to be characteristic of more intense fires.

We initially thought that a few larger smoke particles were responsible for the strong returns in the lidar backscatter data, because of the strong dependence of scattering efficiency on particle radius r ($\propto r^4$ for scattering efficiency, or $\propto r^6$ for backscatter cross section, where $r < \lambda/2\pi$ for Rayleigh scattering and λ is the wavelength of the transmitted signal). Because the large particles in the smoke distribution were in the Mie-scattering regime, we performed Mie-backscattering calculations using the distributions in Fig. 1. The results, shown in Fig. 2b, were that the backscattering came from a broad range of particle sizes with diameters between 0.1 and 30 μm, and that the maximum backscatter was from particles of about 1 μm. Thus, the conclusion was that the strong lidar backscatter returns were primarily from the 0.5–2-μm particles, although both the massive numbers of submicron particles and smaller numbers of larger ones emitted from the fire also contributed.

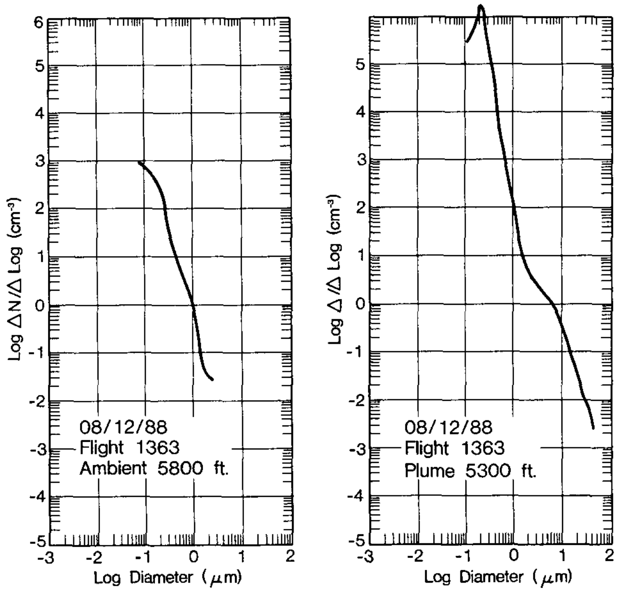

FIG. 1. Particle-size distributions of aerosol particles measured by the University of Washington Convair aircraft sampling system on the day of lidar measurements. (a) Background distribution outside the smoke plume. (b) Aerosol-size distribution within the smoke plume.

A breakdown of the contributions to backscatter by size range (Table 2), both for the dustlike background aerosol and for the carbonaceous smoke and ash particles, quantifies these relationships. Nearly all the calculated backscattering of 2×10^{-9} m^2 m^{-3} sr^{-1} (m^{-1} sr^{-1}) for the background aerosols arose from the few largest sizes that were measured in the 0.9–2.2-μm-diameter regime, which is consistent with the normal, clear-air situation described by Post (1978). For smoke the backscatter in each subrange greatly exceeded the total background amount, and its total backscatter of nearly 6×10^{-7} m^{-1} sr^{-1} was almost 300 times greater than the background.

2) LIDAR SCANS

The lidar system has the capability to scan horizontally and vertically. Full 360° horizontal scans at ele-

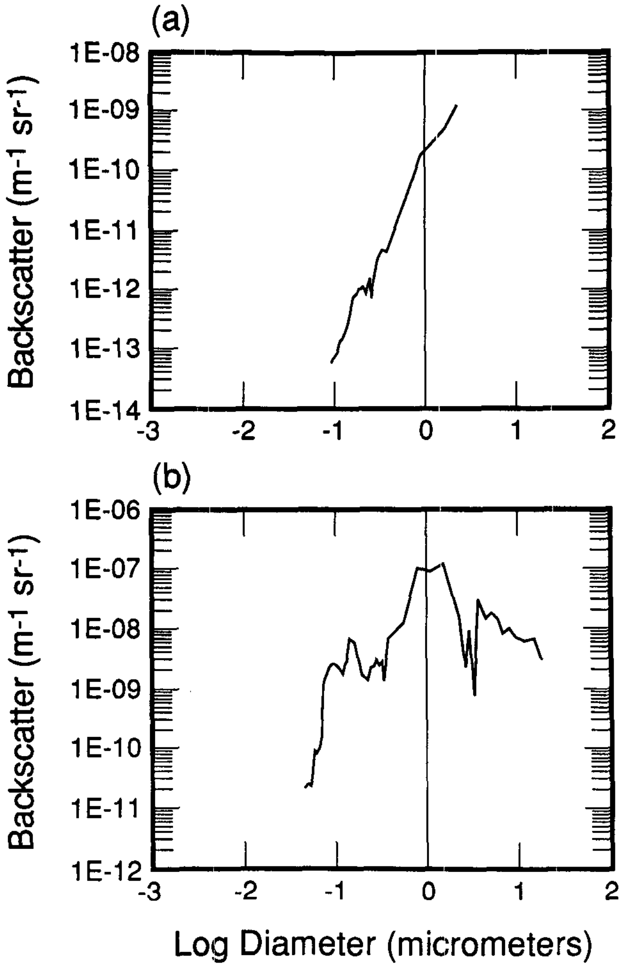

FIG. 2. Mie calculations of lidar backscatter versus logarithm of particle diameter for particle distributions shown in Fig. 1, for (a) the ambient-air distribution outside the smoke plume and (b) the smoke-particle distribution inside the smoke plume.

vation angles greater than zero actually represent cones of data in the atmosphere centered on the lidar scanner. The circular display of these data is referred to by the radar community as a plan position indicator (PPI) display, and the scans are called PPI scans. Full conical scans can be used to determine vertical profiles of the mean horizontal wind using the VAD technique described by Browning and Wexler (1968). Scans in which the elevation angle varies and the azimuth is fixed, called range–height indicator (RHI) scans in radar terminology, represent vertical slices of data from the atmosphere.

Three-dimensional volumes of data can be obtained either by performing PPI sector scans back and forth in azimuth while incrementing in elevation at the end of each sweep ("horizontal" raster scans), or by performing elevation sweeps up and down while incrementing in azimuth (vertical raster scans). We analyzed these scan volumes first by interpolating the lidar data, originally in spherical coordinates, to Cartesian coordinates, and then by using the CEDRIC analysis package that was developed for analyzing Doppler radar data (Mohr and Miller 1983; Mohr et al. 1986). The interpolation necessarily produced some smoothing of the data, and the Cartesian data were further filtered to provide smooth analyzed fields.

The most common horizontal raster scans performed during the Battersby burn consisted of sectors from 200° to 260° azimuth starting at 4° elevation. These scans went up to 7° or 9° elevation at 1° increments, and occasionally the scans were started at 2° or 3° elevation. Scanning parameters were chosen to provide 1° angular resolution in both azimuth and elevation, which gave 122-m resolution at a range of 7 km. The horizontal raster scans were analyzed by interpolating to a 200-m × 200-m Cartesian grid on level surfaces 0.4, 0.5, and 0.6 km AGL, where the reference ground level is the level of the lidar.

We performed vertical raster scans four times during the burn to obtain complete volumes of data around the convection column and smoke plume. These scans consisted of vertical sectors from 2° to 41.5° or 50° elevation, every 1.67° of azimuth from 205° to 250° (azimuth). Scan parameters gave 1.67° resolution in azimuth and elevation, which gave 200-m resolution at a range of 7 km.

3) VELOCITY DATA PROCESSING

For the cross sections shown in this study, we did not analyze the vertical scan sequences as a volume, but instead we analyzed the individual vertical scans by interpolating data from each scan to a Cartesian range versus height grid with 50-m × 50-m resolution. Keeping the Cartesian interpolation plane coincident with the plane of observation resulted in the direction of the radial wind component u_r being within the plane. This wind field can be used to estimate the divergence of u_r. We can then arrive at a value for the vertical wind component w by continuity, as described by Mohr et al. (1986).

TABLE 2. Integrated 10.59-μm backscatter for three aerosol-size categories: Mie calculations using two observed size distributions

	Background		Smoke	
Diameter (μm)	β (m^{-1} sr^{-1})	Percentage	β (m^{-1} sr^{-1})	Percentage
0.1–0.7	3.3×10^{-11}	2	5.9×10^{-8}	11
0.7–5.0	1.97×10^{-9}	98	4.0×10^{-7}	68
5.0–36.0	0	0	1.3×10^{-7}	21
Total	2.0×10^{-9}		5.9×10^{-7}	

Note: Complex refractive indices used for background aerosol (dustlike) and smoke aerosol (carbonaceous) were 1.62–i0.12 and 1.8–i0.7, respectively.

The procedure just outlined neglects the tangential divergence and thus underestimates the actual *w* probably by about half when the convection column is vertical and cylindrical. This is because, under nearly calm low-level wind conditions, convergence of air into the convection column comes from many sides, and the tangential divergence should normally be about equal to the radial divergence. Inflow data from experimental fires, presented by Palmer (1981), indicate that inflow patterns are not always cylindrically symmetric. What is required, however, is that two orthogonal components of the convergence into the convection column be of similar magnitude. This seems to be a reasonable approximation for a vertical column under light wind conditions, neglecting unusual effects such as topographic channeling of the inflow.

4) LOCALE

The lidar scanned from a position just less than 7 km northeast of the center of the burn site. The lidar was at an elevation of 442 m MSL, and the burn area was somewhat lower, mostly near 425 m MSL. The burn region is hilly, with some lower marshy regions of 410 m MSL but also some hills that reach to the level of the lidar. A 457-m MSL ridge between the lidar and the burn site prevented the lidar from scanning down to the base of the fire. The lowest horizontal sector scans were at 2° elevation, which translated to about 245 m above lidar level at a range of 7 km. The burn area was very roughly a rectangle, 3 km north–south by 2.5 km east–west. Ignition, accomplished by helitorch (helicopter), began in the northeast corner (i.e., the downwind corner and the corner closest to the lidar) and proceeded throughout the afternoon. Thus, the fire began about 5 km from the lidar and burned at greater distances from the lidar as the ignition proceeded.

4. Radar results

Debris and ash rising in the plume of the fire in Left Hand Canyon, Colorado, were easily detectable by WPL's X-band radar. Strengths of the signals near the plume source were more than 20 dB above the minimum detectable signal at a range of 28 km. The hodograph (Fig. 3) representing the wind profile above the radar site was obtained from a VAD analysis of a 61° elevation scan at 2226 UTC (1626 MDT) on 10 September. It shows westerly flow of 7–10 m s^{-1} between 0.2 and 2.0 km AGL, and a jet of 13 m s^{-1} just below 1 km AGL. There is a decrease of winds with height between 1 and 2 km above the radar. According to Byram (1954) and Aronovitch (1989), this indicates the potential for buoyancy-dominated or blowup fire behavior. The observed behavior of the plume was clearly wind driven, however, during the period of the radar observations.

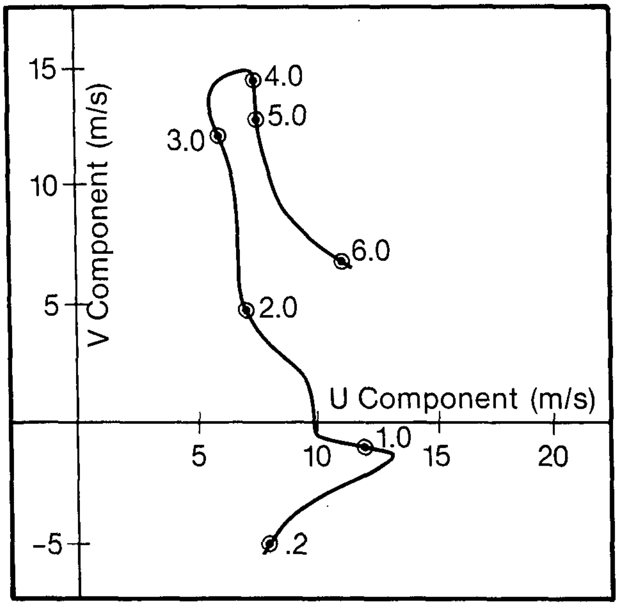

FIG. 3. Hodograph of horizontal winds measured by the WPL 3.2-cm radar at 2226 UTC 10 September 1988, using the VAD technique. Each dot represents the end of a velocity vector (with tail at the origin), and numbers next to dots are heights (km AGL) of the wind observation.

Figure 4 (top) shows a horizontal cross section of u_r within the plume at a height of 1 km above radar (or about 0.5 km above the fire) at 1632 UTC. The direction of the radar beam was less than 30° off the plume axis direction, so these data show the approximate along-axis wind component within the plume. A notable feature in the figure is the well-defined minimum in the magnitude of u_r along the plume axis and a significant increase in the magnitude of the velocity component at the plume edge. Velocity magnitudes are less than 6 m s^{-1} near the plume axis, and they increase to greater than 13 m s^{-1} along either edge. This pattern implies that the convection column consisted of a vortex pair, with two counterrotating horizontal vortices (rolls) oriented along and on either side of the plume axis, and the updraft along the plume centerline. This is a type I vortex according to McRae and Flannigan's (1990) classification. Upward motions within the buoyant plume transport weak horizontal momentum from near the surface into the plume center, while strong westerly momentum is brought down from upper levels by the descending branches of the rolls (as shown by the effects on the plume edge). A horizontal slice through a smoke plume showing slower air in the middle of the plume and faster air at the edges thus represents the signature of a counterrotating vortex pair.

The ambient flow was strong compared with Church et al.'s (1980) criteria for counterrotating rolls. This

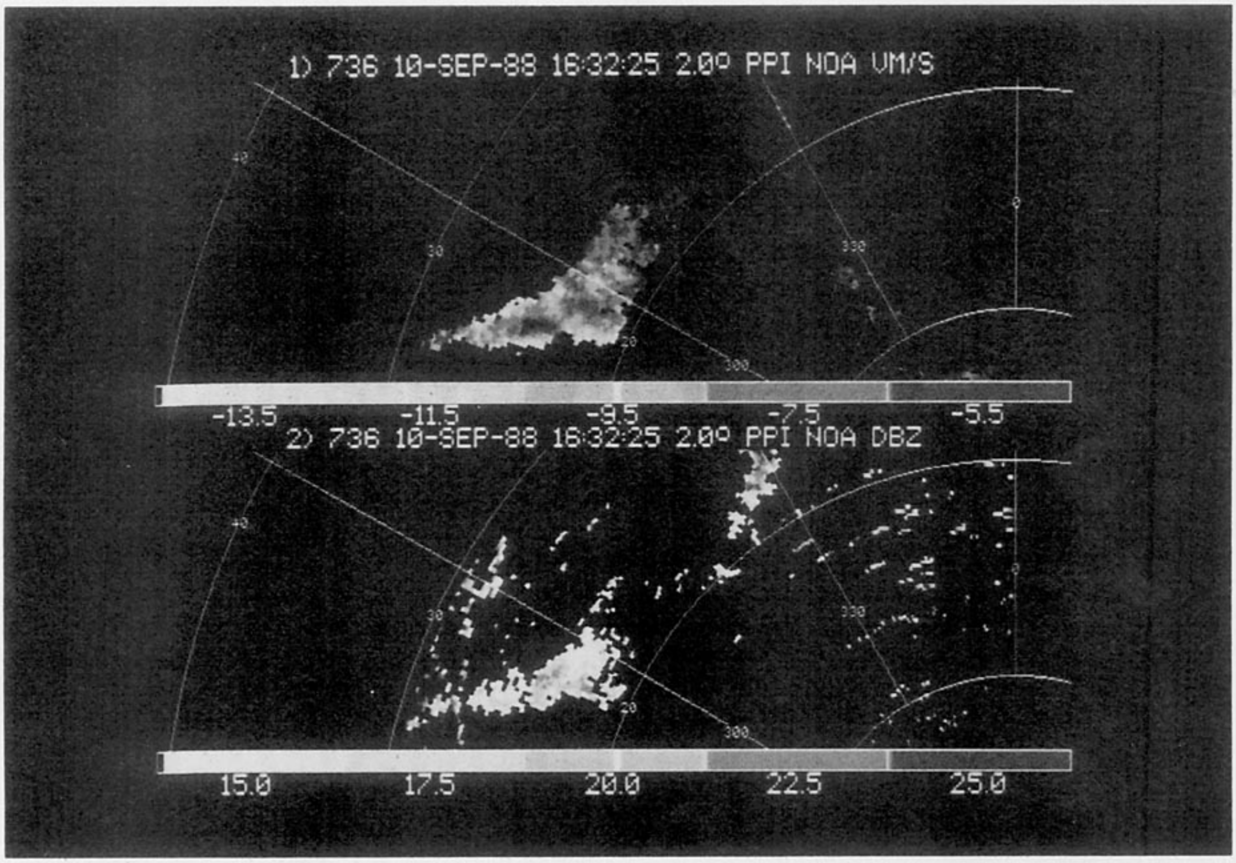

FIG. 4. Radar observations at 1632 UTC of the smoke column emitted by the Left Hand Canyon fire on 10 September 1988. Observations are from a horizontal sector scan at 2° elevation angle. Range rings are at 10 km, and azimuth markers at 30° intervals. Top: u_r plot; velocities approaching the radar are negative. Wind speeds along the centerline of the plume are lighter, and wind speeds at the edges are stronger. Bottom: Radar backscatter (dBZ, a different dB scale from the lidar measurements).

indicates that the upwind topography, a mountain barrier, probably influenced the structure of the convection column. This could have occurred either by reducing the local ambient flow over the fire or by causing the aerodynamics of the flow over the ridge to contribute to vortex production.

Observed values of radar reflectivity (Fig. 4, bottom) were between 10 and 20 dBZ within the plume. Reflectivity values of this magnitude are much too large to be caused by scattering from micrometer-sized smoke particles and are most likely caused by ash particles or other debris (1-mm to 1-cm diameter) carried aloft by the buoyant updraft. Vertical cross sections showed that the plume did not rise above the 2-km level.

Information about the shape of the scatterers was provided by our polarization measurements. Unexpectedly, we found very large values of CDR (near 0 dB) within the plume, suggesting that the scatterers had a flat, needlelike appearance as viewed from the perspective of the radar (see section 3a). This is more than 20 dB greater than values observed on this day for spherical liquid water cloud droplets in other areas of these scans away from the plume. Radke (1990, personal communication) has pointed out to us that "biomass fires often produce a significant concentration of millimeter-sized ash particles which have a largely platelike symmetry." The observed CDR values could alternatively have been produced by scattering from pine needles or needlelike fibers swept up into the plume by the strong updraft. Radke has also observed that "needle-like objects have seldom been seen in PMS (Particle Measurement Systems probes) optical imaging taken in more than a dozen large fires." However, millimeter-sized needles would have to be present in only very low concentrations to produce these kinds of radar returns, and such infrequent scatterers could easily evade PMS sampling. Thus, the measurements could have been produced either by platelike ash particles that were viewed edge on by the radar or by pine needles or other needlelike objects even if the latter were present only in low concentrations.

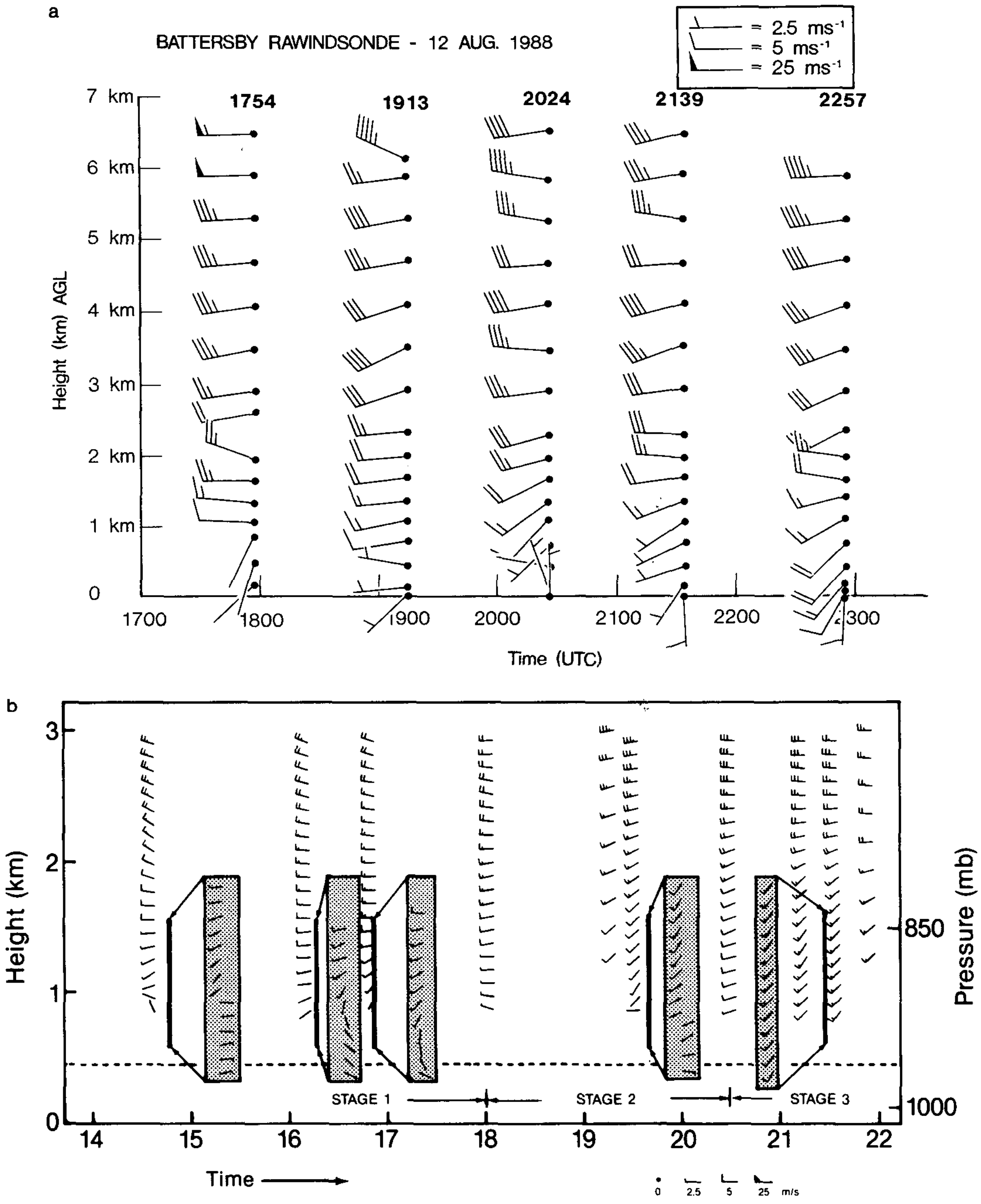

FIG. 5. Vertical profiles of the horizontal winds determined (a) by rawinsonde ascents from the lidar site (Radke and Locatelli 1988), and (b) by lidar scans processed using VAD techniques. VAD profiles are from scans at 10° elevation angle; supplementary 5° scans are expanded and boxed. Times (UTC) and vertical extents of 5° scans are indicated by bold vertical lines. Durations of the three stages in the burn are indicated at the bottom of the VAD plot. The time coordinate reads from left to right.

5. Lidar results

The lidar obtained strong return signals from the smoke column and plume for the duration of the Battersby Township burn. The morning weather was sunny, warm, and humid. Solar heating of the surface produced an unstable, convective, atmospheric boundary layer (ABL) by noon, which evolved into a subcloud layer as cumulus clouds formed in the afternoon and which changed back into an unstable, convective ABL as cloud activity diminished later in the afternoon. For convenience we refer to this afternoon

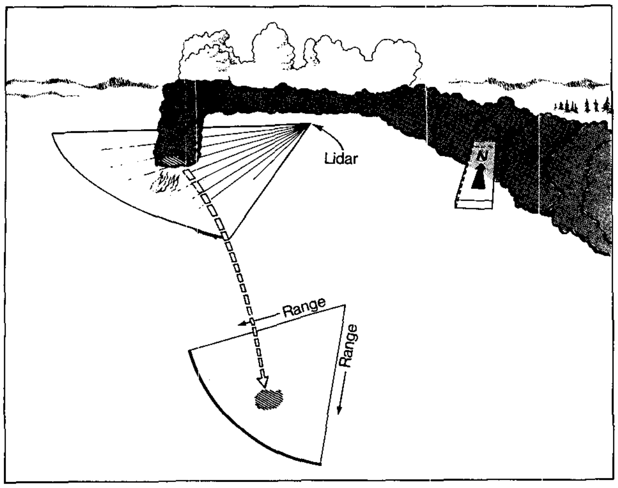

FIG. 6. Horizontal cross section at 6.1° elevation through the base of the convection column at 1732 UTC, less than a half hour after the first ignitions. (a) Schematic drawing of the horizontal scan through the ascending column; the resulting backscatter from the lidar scan is represented in the lower part of the drawing. (b) Lidar backscatter from the horizontal scan described in (a). North is up and west to the left, and the lidar was located in the upper right of the figure where the radials converge. The dark, high-backscatter region representing the smoke column is thus southwest of the lidar and at a range of approximately 5 km (as shown in Figs. 7 and 8).

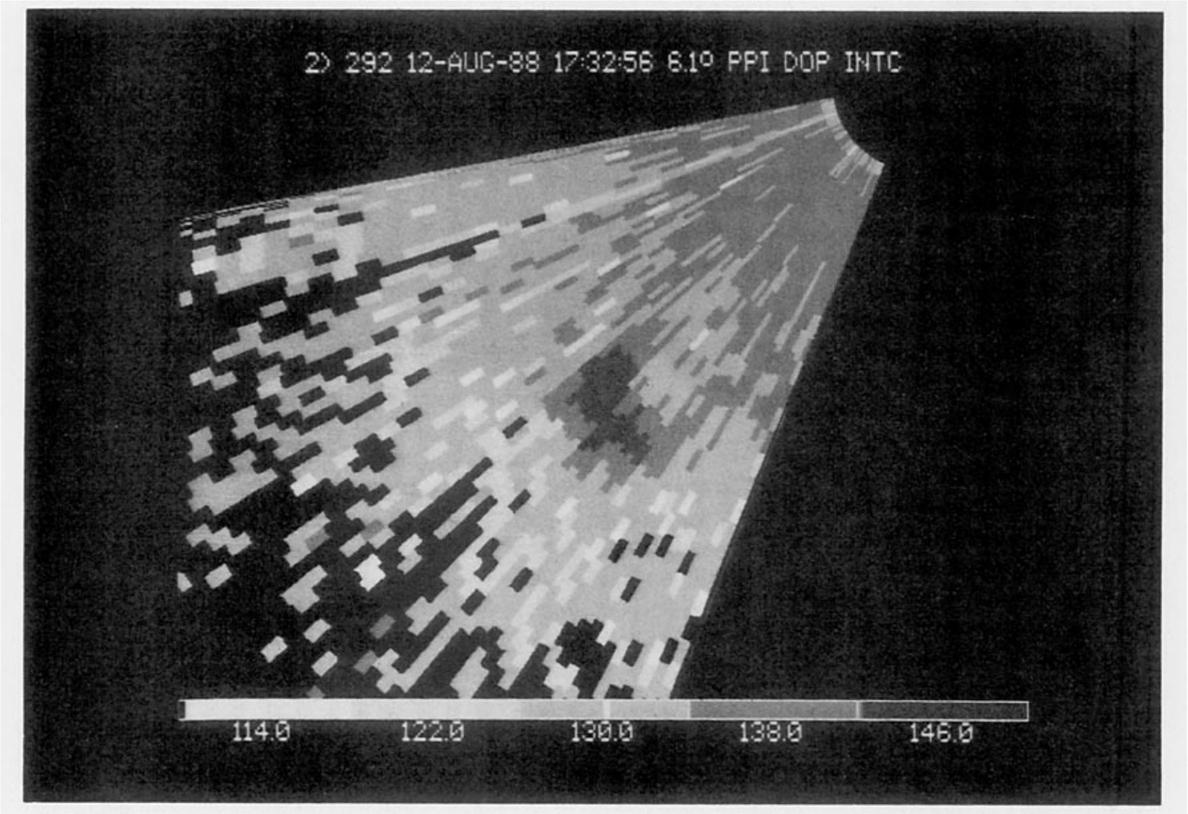

ABL or subcloud layer as the *mixed layer* in this paper even though the layer is not always *well* mixed in the vertical or horizontal.

It was obvious during the course of the afternoon that the meteorological background was changing considerably. We identified three stages in the evolution of the mixed layer on the afternoon of 12 August. The three stages were identified from the radiosonde wind profiles (Fig. 5a), from the lidar VAD wind profiles (Fig. 5b), and from the behavior of the smoke column and plume indicated in the lidar images, some of which are presented later in this paper (Figs. 6–14).

The first stage occurred during and prior to the first hour (1700 UTC) of the burn. The mixed layer was very moist with dewpoints exceeding 22°C (70°F), and the winds were variable in direction and very light below about 1.5 km AGL, and westerly above. The smoke column responded to these conditions by rising straight up for 1.5 km, then shearing off to the east at higher levels. The smoke column also produced vigorous cumulus activity as a result of the high moisture content of the mixed layer.

The second stage was a time of transition between the first stage and the third stage. Winds in the lower mixed layer were stronger than during the first stage, but still variable in direction, although they tended toward southwesterly. A lidar VAD wind profile taken at 1939 UTC, in fact, showed easterly flow below 600 m AGL. Much of this wind variability resulted from cumulus congestus activity, and brief rain showers in the form of a few large drops fell at the lidar site during this phase. In the upper part of the boundary layer above 1 km AGL, the flow turned southwesterly, and this southwesterly flow tended to penetrate farther and farther down into the boundary layer as the afternoon proceeded.

The third stage occurred during the last half hour of the burn (after about 2030 UTC or 1630 LST) and during the hour of observations after ignitions ceased, when the southwesterlies reached the surface. Westerly winds continued above 2 km AGL. The subcloud layer dried, and cumulus activity diminished until after 2300 UTC (1900 LST).

Later in the evening strong thunderstorm rains began to fall. Widespread rainfall then persisted through the night.

a. Early stage

1) LIDAR BACKSCATTER

Lidar backscatter data during the early phase of the burn show the convection column rising vertically to nearly 1.5 km, and the plume being carried to the east at higher levels. The sketch in Fig. 6a shows the rise of the plume during this stage, and Fig. 6b shows a horizontal cross section of lidar backscatter intensity through the base of the column. Figure 7a is an analysis of the backscatter field interpolated to a level surface 0.4 km above the level of the lidar, as described in section 3b.2. Backscatter values (dB) are proportional to the backscatter cross section (m^{-1} sr^{-1}). High values of aerosol backscatter (shaded) correspond to the core of the convection column. Figure 7b shows the Doppler radial velocity pattern also interpolated to the 0.4-km-level surface; this field is described in greater detail in the next subsection.

A vertical cross section of lidar backscatter through the convection column (Fig. 8a), analyzed on a Cartesian grid from a vertical raster scan, shows the column rising to a height of approximately 1 km. Above this height the plume broadens somewhat and comes "out of the page" in the westerly flow above 1.5 km. The dropout of signal above 2 km at ranges greater than 5 km indicates shadowing by liquid water in the vigorous cumulus activity atop the updrafts of the fire. The cloud

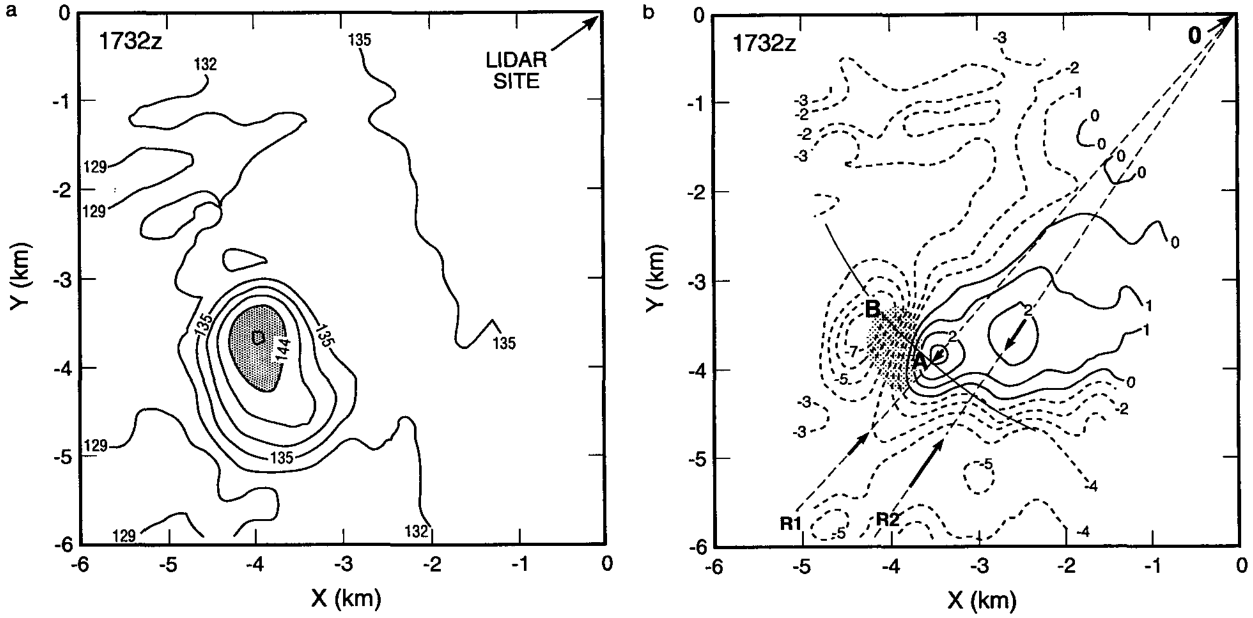

FIG. 7. Horizontal cross section at 400 m AGL through the base of the convection column at 1732 UTC. The x and y values are kilometers east and north of the lidar site at (0, 0). (a) Backscatter (dB) with contours at 3-dB intervals and the region greater than 144 dB shaded. (b) Radial wind u_r (m s^{-1}) contoured at 1 m s^{-1} intervals. Negative values are toward the lidar, and positive values away. The shaded region corresponds to the shaded region in (a). Lines O–$R1$ and O–$R2$ are radials from the lidar site showing velocity convergence to the east of the fire, and arc AB is a segment of a circle centered at the lidar.

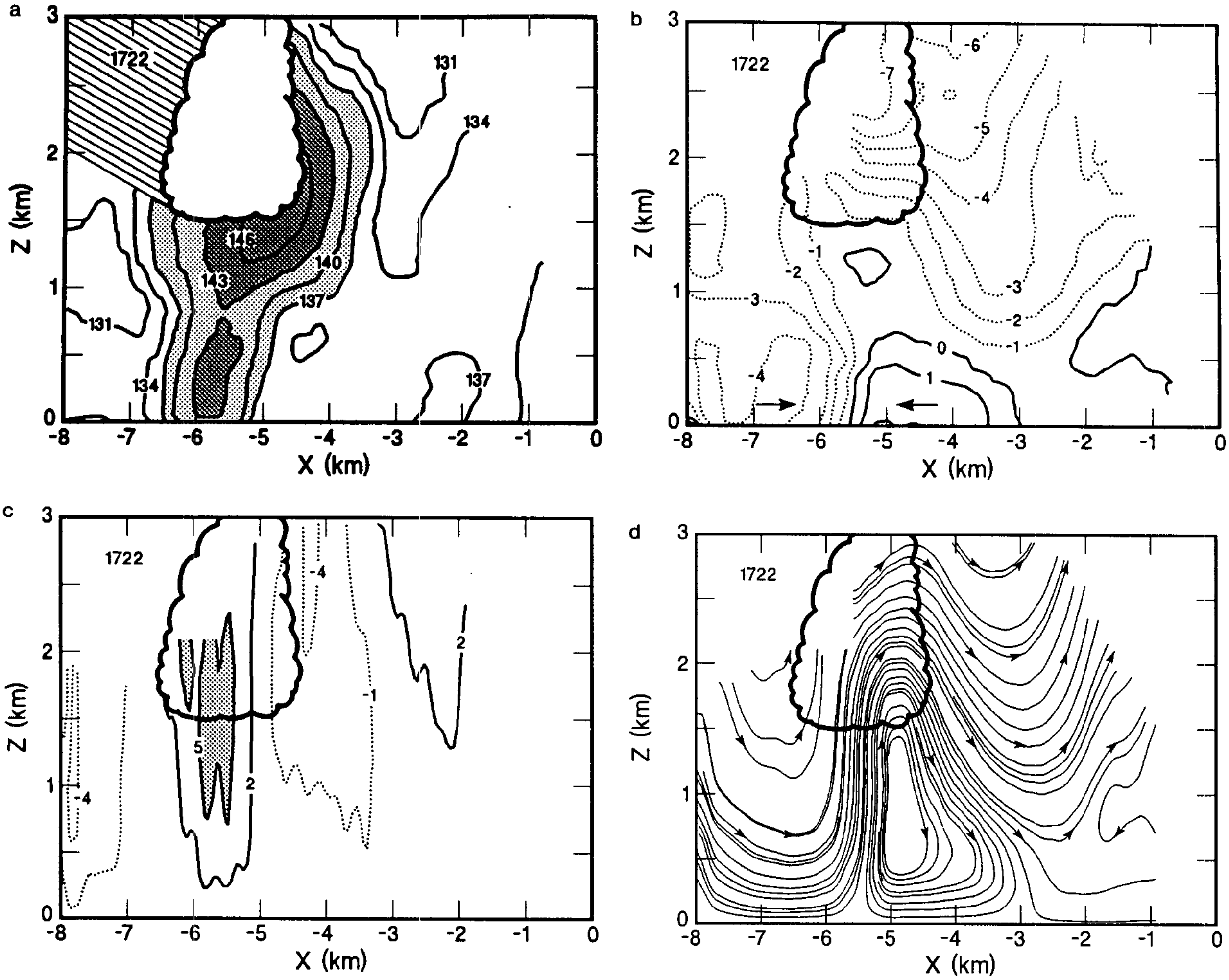

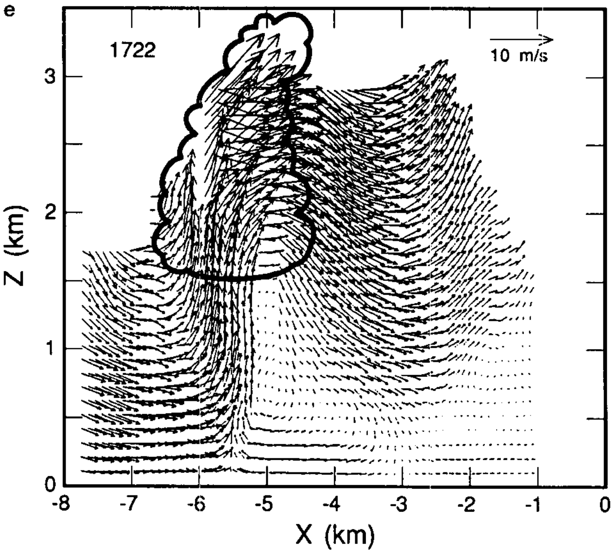

FIG. 8. Vertical cross section at 1722 UTC along the 223.4° azimuth radial from the lidar, which was located at the origin (0, 0) in the figure. (a) Backscatter (dB) contoured at 3-dB intervals. The region greater than 137 dB is indicated by light shading, and the region greater than 143 dB, by heavy shading. The cloud (bold scalloped outline) was determined subjectively from the backscatter pattern, and the hatched area behind the cloud represents the region blocked by the cloud. (b) u_r (m s^{-1}) at intervals of 1 m s^{-1}. Positive values indicate flow away from the lidar; negative values, toward. Arrows indicate the convergence region below the cloud. (c) Analysis of w (m s^{-1}) determined from divergence of u_r, with contours at 3 m s^{-1} intervals. The region with w greater than 5 m s^{-1} is indicated by shading. The peak value observed in this region was 7.5 m s^{-1} above cloud base. (d) Two-dimensional streamlines of flow and (e) two-dimensional wind vectors in the vicinity of the convection column determined from the u_r and w fields in (b) and (c).

was drawn where the backscatter first dropped off significantly. As discussed in section 5b, some of this attenuation could have resulted from the swelling of hygroscopic aerosols at the high relative humidities near the cloud. Thus, the cloud may have actually been somewhat smaller than portrayed.

PPI scans at 20° elevation angle (not shown) indicate that the smoke plume started 5 km southwest of the lidar site and was carried to the south of the site by the westerly flow, at a range of 4 km; the beam at this range is 1.45 km above the ground. A cross section of this portion of the smoke plume (Fig. 9) shows that it spread out laterally and extended back somewhat toward the lidar (to the right in Fig. 9b). The signal dropout above the plume in this figure again indicates cumulus cloud activity with cloud base at about 2 km AGL.

2) DOPPLER WINDS

The lidar also provided data on the velocity structure in and around the convection column. Figure 7b shows the Doppler radial velocity u_r field analyzed on the Cartesian grid at 0.4 km AGL. A distinct convergence pattern is evident along rays *O–R*1 and *O–R*2, as indicated by the arrows, and in the wind field to the east of the arrows. This convergence line to the east of the column is undoubtedly related to the downwind line of cumulus congestus clouds that formed in this region.

The rotational signature in a horizontal display of the radial wind (such as Fig. 7b) consists of flow toward the lidar next to flow away from it, at the same radial distance from the lidar. Figure 7b shows such a signature between points *A* and *B*, which are on opposite sides of the convection column (shaded oval). This pattern shows that the entire vertical column was rotating [i.e., that this was a type II vortex according to McRae and Flannigan's (1990) classification].

Video (VCR) recordings of the smoke column from the lidar site revealed strong anticyclonic (clockwise) rotation of the entire column during the first stage of the burn, and more moderate anticyclonic rotation at times later in the burn. Estimates of the early rotation rate from the video were one revolution in 5 min, for an angular velocity of 0.02 rad s^{-1}. Angular velocity and vorticity were also estimated from the lidar data: flow toward the lidar exceeding 7 m s^{-1} is shown in Fig. 7b near point *B*, and flow away from the lidar of more than 4 m s^{-1} occurs near point *A*. The centers of these maxima are separated by about 750 m, indicating a vorticity of 0.02 s^{-1}. The angular velocity is estimated to be 0.01 rad s^{-1}, using the solid-rotation result that vorticity is twice the angular velocity (e.g., Hess 1959, p. 211). The agreement between the two methods is good, considering that the velocity fields in Fig. 7b have been smoothed (estimates of angular velocity from unsmoothed velocity fields were 0.02 rad s^{-1}, in even closer agreement with VCR estimates).

A vertical cross section of u_r (Fig. 8b) shows a region of convergence nearly 2 km deep below the upwind side of the base of the cloud. As described in section 3b.3, one can calculate the divergence field and an estimate of the vertical velocity w field from a radial range–height cross section of u_r (Fig. 8c). Using these u_r and w values, one can then plot two-dimensional velocity vectors and streamlines using the CEDRIC software package. The streamline field (Fig. 8d) and the velocity vector field (Fig. 8e), obtained from the u_r

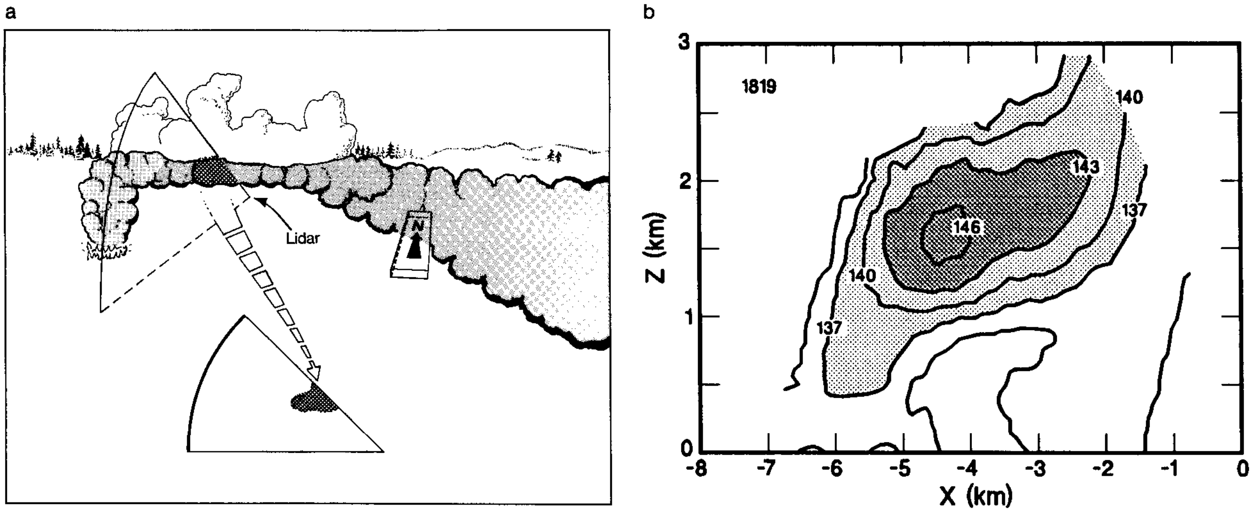

FIG. 9. Vertical cross section (RHI) of the smoke plume at 1819 UTC at 215° azimuth from the lidar. (a) Schematic drawing of the relationship between the smoke plume and the lidar RHI scan. (b) Analysis of backscatter (dB) at 3-dB intervals. The region greater than 137 dB is shaded lightly, and the region greater than 143 dB shaded heavily. Clouds (not shown) were between $x = -3$ and -6 km, with bases between $z = 1.5$ and 2 km.

field in Fig. 8b, show a nearly vertical updraft into the convection column. The ambient flow, light at levels below 0.5 km, blew generally from southwest to northeast (left to right in the figure), and therefore downwind of the updraft is a region of strong subsidence. Farther downwind is another region of rising motion representing a gravity-wave response with a wavelength of approximately 3.5 km. Upwind of the fire, at the left edge of the figures, is a strongly subsiding inflow region similar to that described by Palmer (1981).

From the w analysis (Fig. 8c), the peak value of upward motion calculated from the radial component of the divergence field was greater than 7.5 m s^{-1} at the base of the cloud. Assuming that the tangential convergence (across the lidar beam) was of similar magnitude, we estimate a peak total w value of 15 m s^{-1} at cloud base. This is still an underestimate, because the lidar could not scan down to the base of the fire where the maximum convergence values probably existed.

Latent-heat-driven updrafts in the deep cumulus clouds that formed over the fire were certainly the major contribution to the strong w observed in the convection column above the fire. Because of the strong relationship among w, convergence, and concentration of environmental vorticity, it is likely that the deep, moist convection also had a strong role in developing and maintaining the whole-column rotation during this phase of the fire.

b. Middle stage

The middle, transitional stage of the burn was characterized by ambient flow that was variable in direction (generally southwesterly to westerly in the boundary layer), occasionally light, and occasionally as strong as 3–4 m s^{-1}, but tending to increase in speed with time. The plume blew generally toward the lidar, and at times we could smell smoke and see large ash particles at the lidar site. A PPI scan taken at 45° elevation angle (not shown) indicated that the lidar site was surrounded by the smoke plume; the backscatter returns were strong out to a slant range of 2.5 km, corresponding to a height of 1.8 km AGL.

At times the winds in the mixed layer were light, as in the early stage. Figure 10 shows that during such a lull, at 1932 UTC, the main convection column went straight up to 1 km. Above this level the stronger southwesterly (left-to-right) flow carried the smoke plume toward the lidar. Downwind of the main updraft a region of general subsidence caused the smoky (high-backscatter) air to descend into the lower mixed layer. As in the cross sections in Fig. 8, the u_r field (Fig. 10b) shows a strong convergence region below the main updraft (between $x = -7$ and -8 km). In this region, at cloud base, the strongest updraft reached 12.0 m s^{-1}. Because this represents a w estimate based on radial divergence, and because the convection column appears cylindrically symmetric at this time, the total peak w is estimated to be 24 m s^{-1}. The streamline and two-dimensional velocity vector analyses (Figs. 10d, e) show a weak updraft (greater than 2 m s^{-1}) entering the base of the secondary cumulus cloud (between $x = -5$ and -6 km) that had drifted downwind of the main updraft, and they also show another region of rising motion, probably a gravity-wave response, between $x = -1$ and -2 km, downwind of the region of general subsidence.

At other times during this stage, mixed-layer winds were stronger and blew the convection column over. A vertical cross section along the longitudinal (centerline) axis of the plume at 2025 UTC (Fig. 11) shows clearly the effect of the change in flow on smoke-column behavior. Instead of rising straight up for a time before being carried horizontally, the column was immediately bent over and carried toward the lidar. Just after this sequence of scans was performed, at 2034 UTC, we noted on our log sheets that large (1 mm to 1 cm) ash particles had been falling at the site for more than 10 min. Horizontal sector scans (Fig. 12) also show that the plume spread horizontally as the winds carried it to the northeast past the lidar. We have not confirmed whether any kind of rotation was present during this phase of the burn.

During this stage of the burn, at those times when the convection column was bent over by the mixed-layer winds (Fig. 11a), w values were lighter than during the previous stage, with peak magnitudes in the updraft reaching 7.8 m s^{-1}, based on the radial divergence (Fig. 11c). Because of the mean flow in this case, the column no longer had cylindrical symmetry, and the tangential divergence was probably less than the radial divergence. Thus, the total peak updraft speed was most likely between 7.8 and 15.6 m s^{-1}, probably near the lower end, that is, probably near 10 m s^{-1}.

Although cloud activity was present at the time of Fig. 11, it was considerably diminished, and the clouds were smaller. Because it was less obvious where the clouds were in Fig. 11, none are indicated, even though some smaller clouds were present.

c. Late stage

Late in the afternoon southerly surface winds and southwesterly flow in the mixed layer carried the plume north and eastward, and when the fire was still active the convection column resembled the bent-over column in Fig. 11. After the fires were no longer being ignited, smoke was still being emitted, and the plume passed to the west and north of the lidar site (Fig. 13). A vertical cross section of the plume to the northwest of the site shows that the smoke was confined to the lowest 1.6 km of the atmosphere (Fig. 14), and the

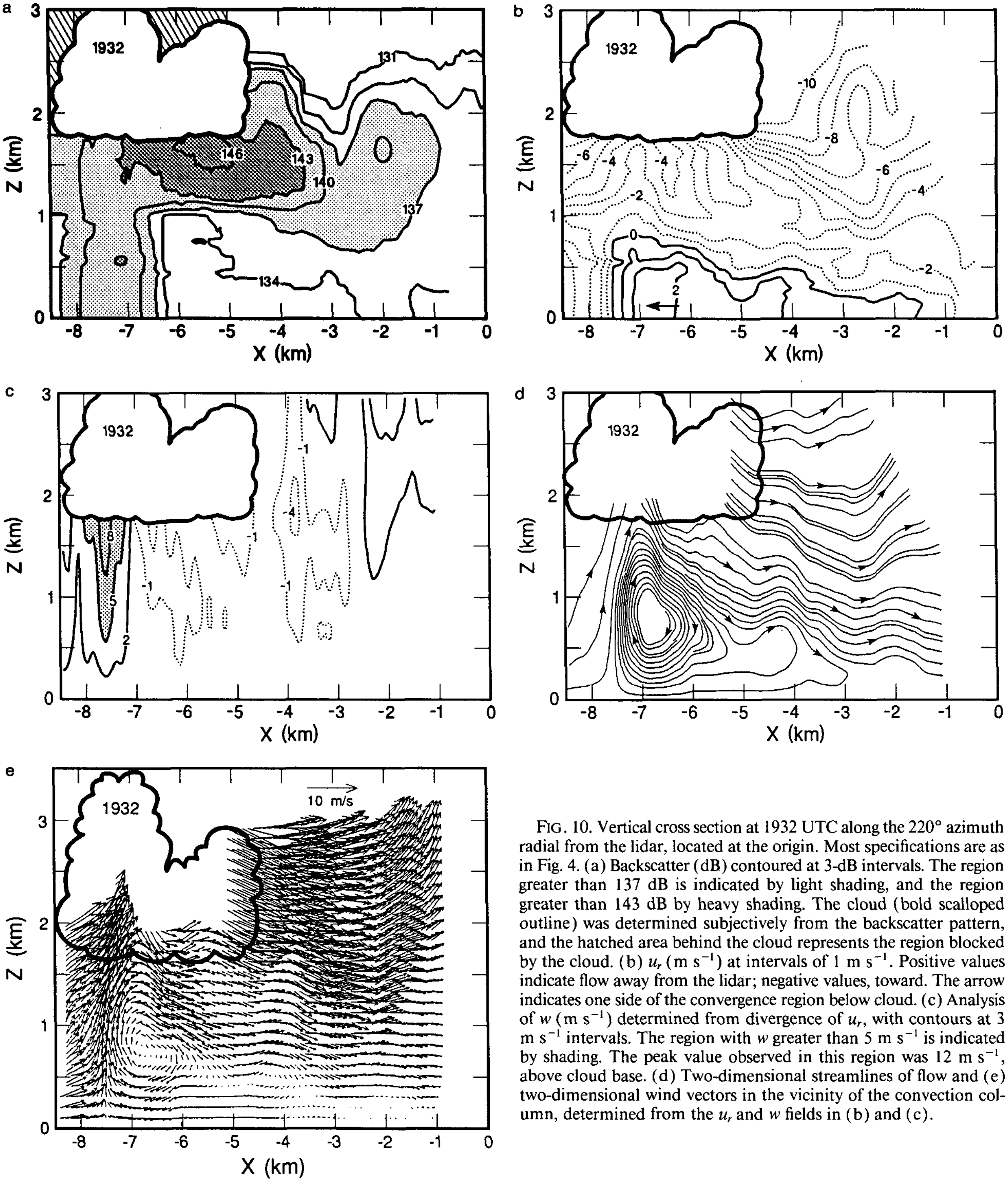

FIG. 10. Vertical cross section at 1932 UTC along the 220° azimuth radial from the lidar, located at the origin. Most specifications are as in Fig. 4. (a) Backscatter (dB) contoured at 3-dB intervals. The region greater than 137 dB is indicated by light shading, and the region greater than 143 dB by heavy shading. The cloud (bold scalloped outline) was determined subjectively from the backscatter pattern, and the hatched area behind the cloud represents the region blocked by the cloud. (b) u_r (m s^{-1}) at intervals of 1 m s^{-1}. Positive values indicate flow away from the lidar; negative values, toward. The arrow indicates one side of the convergence region below cloud. (c) Analysis of w (m s^{-1}) determined from divergence of u_r, with contours at 3 m s^{-1} intervals. The region with w greater than 5 m s^{-1} is indicated by shading. The peak value observed in this region was 12 m s^{-1}, above cloud base. (d) Two-dimensional streamlines of flow and (e) two-dimensional wind vectors in the vicinity of the convection column, determined from the u_r and w fields in (b) and (c).

radiosonde sounding taken at 2039 UTC indicates that this was the top of the mixed layer. Thus, during this last stage of the burn, when the fire was probably smoldering, the smoke column had little buoyancy, and the plume was confined to the mixed layer.

d. Aerosol detection

A final issue related to aerosol-size distribution as seen by the lidar is the presence of backscatter maxima near the clouds in Figs. 8a and 10a. A likely mechanism

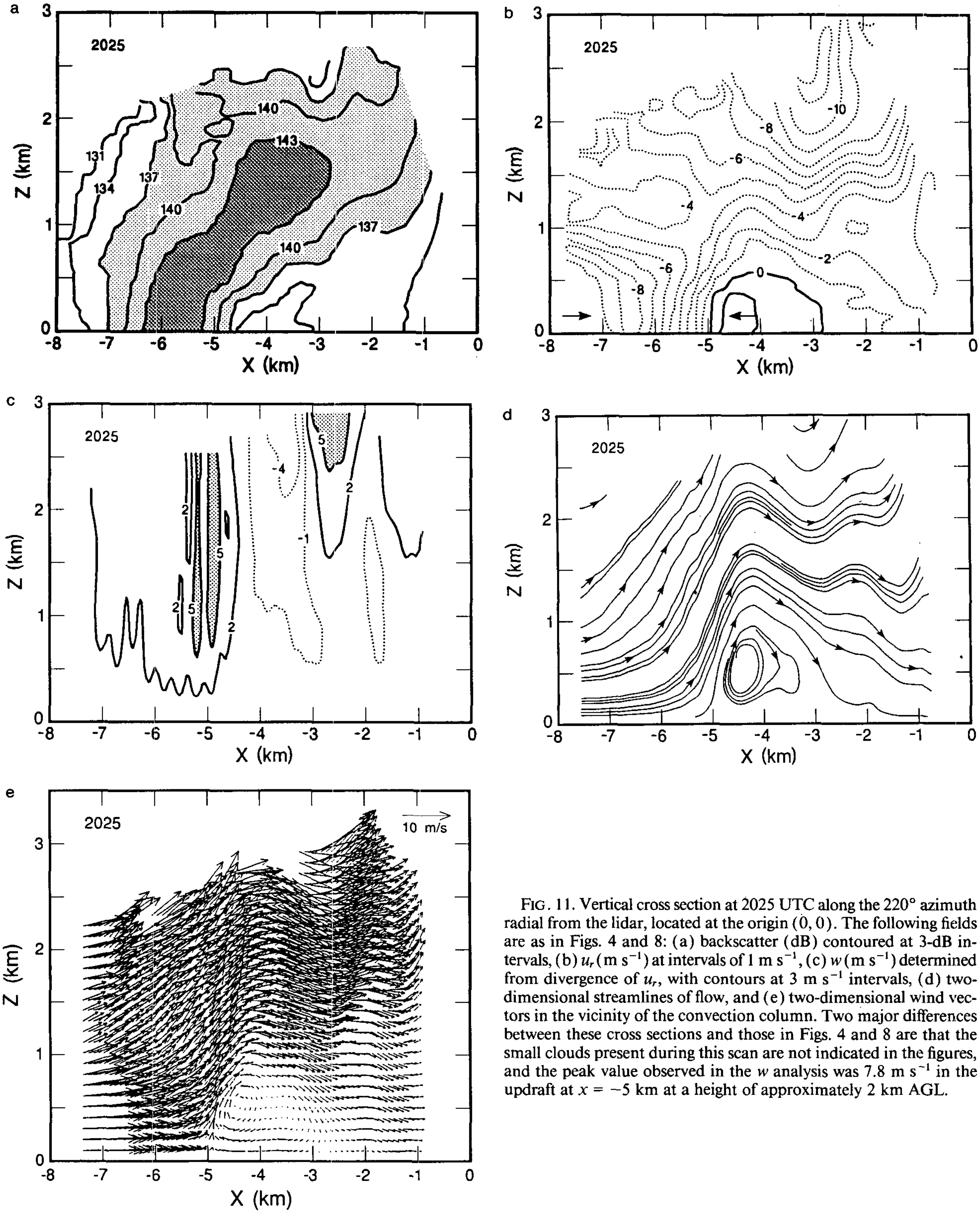

FIG. 11. Vertical cross section at 2025 UTC along the 220° azimuth radial from the lidar, located at the origin (0, 0). The following fields are as in Figs. 4 and 8: (a) backscatter (dB) contoured at 3-dB intervals, (b) u_r (m s^{-1}) at intervals of 1 m s^{-1}, (c) w (m s^{-1}) determined from divergence of u_r, with contours at 3 m s^{-1} intervals, (d) two-dimensional streamlines of flow, and (e) two-dimensional wind vectors in the vicinity of the convection column. Two major differences between these cross sections and those in Figs. 4 and 8 are that the small clouds present during this scan are not indicated in the figures, and the peak value observed in the w analysis was 7.8 m s^{-1} in the updraft at $x = -5$ km at a height of approximately 2 km AGL.

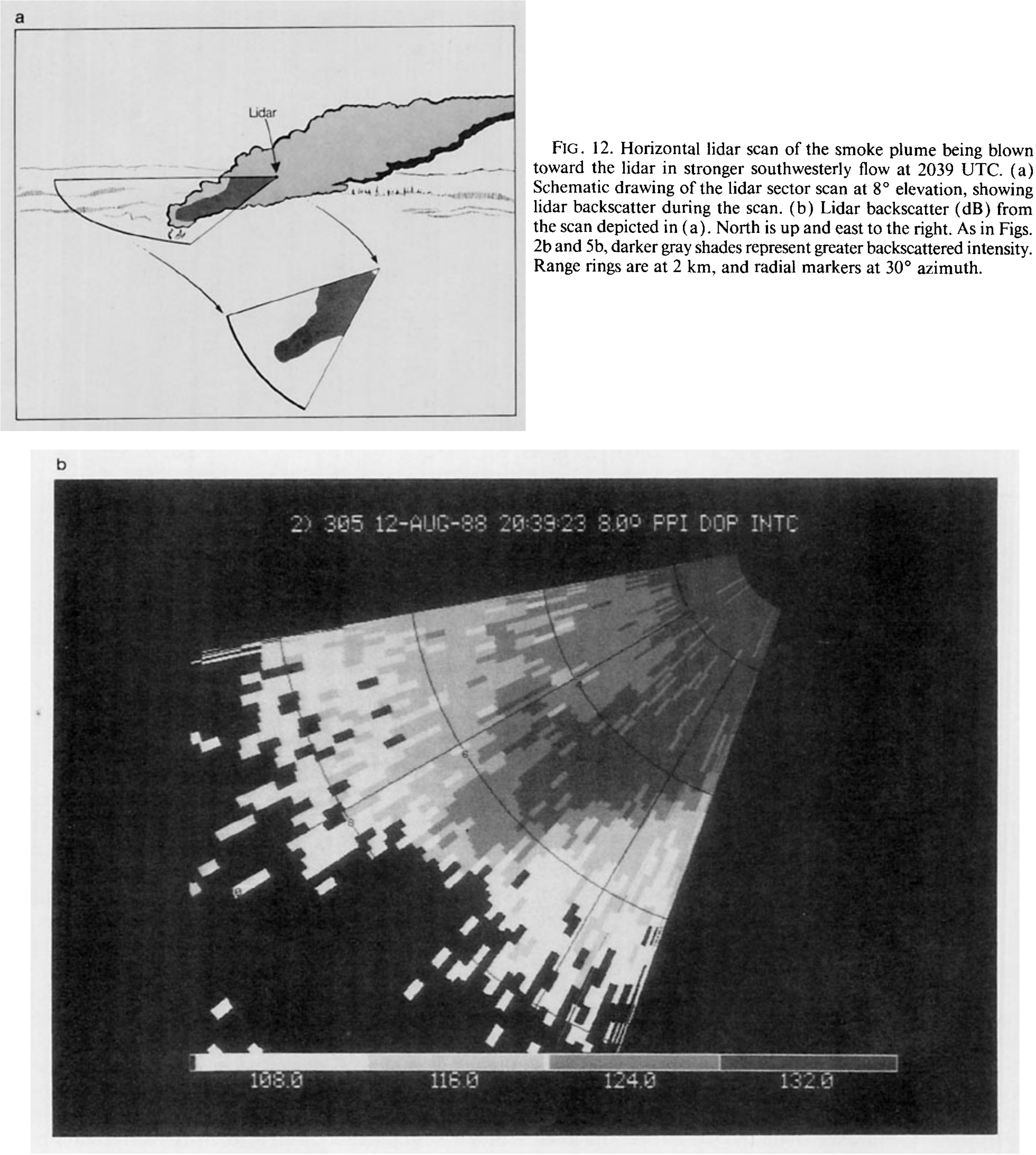

FIG. 12. Horizontal lidar scan of the smoke plume being blown toward the lidar in stronger southwesterly flow at 2039 UTC. (a) Schematic drawing of the lidar sector scan at 8° elevation, showing lidar backscatter during the scan. (b) Lidar backscatter (dB) from the scan depicted in (a). North is up and east to the right. As in Figs. 2b and 5b, darker gray shades represent greater backscattered intensity. Range rings are at 2 km, and radial markers at 30° azimuth.

for this effect is the swelling of hygroscopic particles at high relative humidities (e.g., greater than 80%; Grund 1990, personal communication). Radke and Hobbs (1991) found evidence of high relative humidities in the vicinity of cumuli, and Hobbs and Radke (1969), for example, documented the presence of such soluble nuclei in forest fire smoke. The swelling produces larger particles in the size distribution, which produce greater backscatter in regions of high relative humidity. These regions include the updraft just before it enters cloud base and the detrainment region immediately downwind of the cloud. Both the updraft and detrainment regions show high backscatter in Figs. 8a and 10a. The high-backscatter areas downwind of the clouds are evidence that at least some smoke passes through the cloud and is detrained back into the atmosphere.

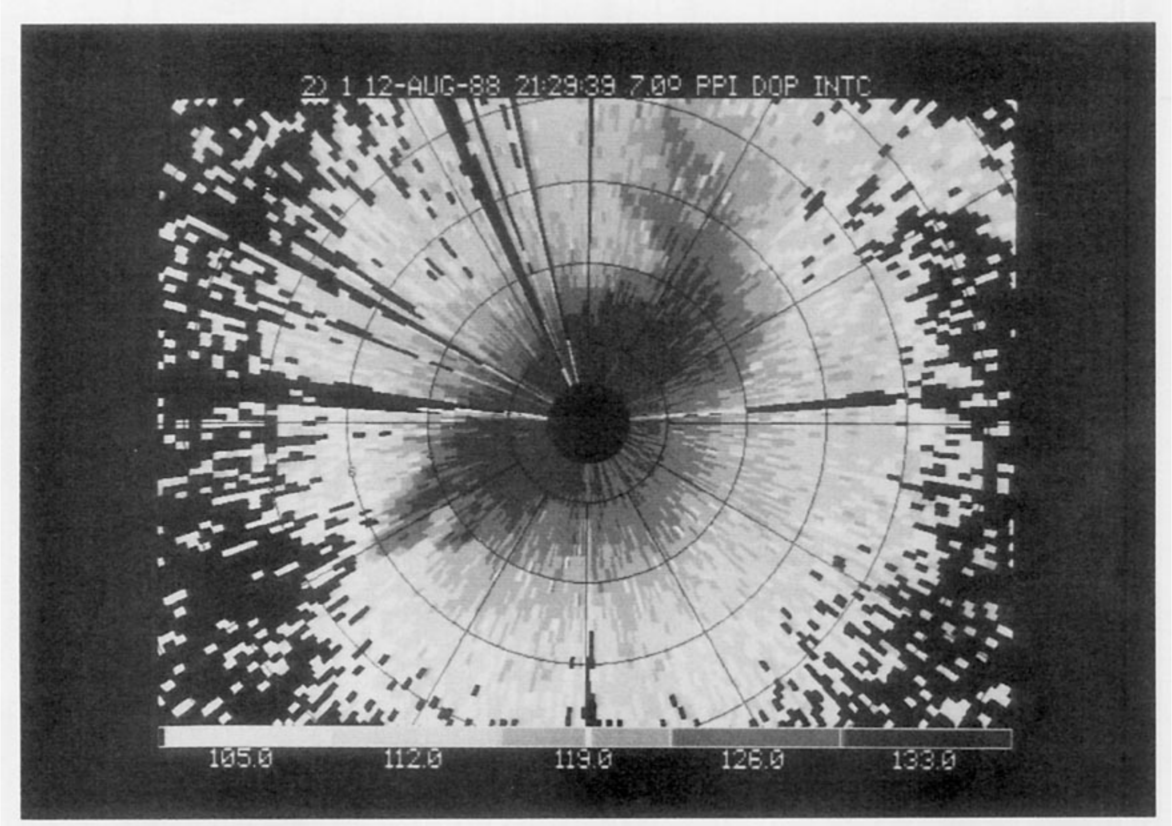

FIG. 13. Quasi-horizontal, conical (PPI) scan at 7° elevation of the lidar backscatter (dB) at 2129 UTC during stage three of the burn. The smoke plume (darker gray shades) began at 6 km and 240° azimuth from the lidar (center of the figure); it passed just to the west and north of the lidar site as it drifted to the northeast.

6. Conclusions

Conditions in Battersby Township on the afternoon of 12 August 1987 were less than favorable for good lidar performance and for the acquisition of a good dataset. The environment was poor for the propagation of IR: high humidities both restricted the maximum range of the lidar during the early stages of the burn to 7 km or less and resulted in widespread cumulus clouds, which further restricted the ability of the lidar to see above the subcloud layer. Furthermore, the meteorological background changed considerably through the period of observation. The convection column, instead of being nearly steady state and thus easy to track and observe, completely changed character as the low-level winds became stronger during the period. In spite of these difficulties the lidar obtained an excellent dataset, and we conclude that under more optimum conditions, the lidar would have obtained an even better case-study dataset.

Using the radar and lidar observations described in this paper, we have addressed two major questions. The first question, on the fate of the smoke emitted by a large fire, was easily addressed by both instruments because of the strong backscatter of the smoke particles in the plumes. The radar was able to track the dispersing of the Left Hand Canyon smoke plume for more than 30 km. It sensed larger particles (millimeter sized), and the predominant particle shape presented to the radar was needlelike, according to the depolarization data. Ash platelets viewed edge on, or needles, even in very low concentrations, are consistent with these radar observations.

The lidar monitored the fate of smoke emissions from a prescribed fire ignited during afternoon hours. Returns were most strongly weighted by the 0.7–5.0-μm smoke particles, although smaller (0.1–0.7 μm) and larger (5.0–36.0 μm) particles also contributed. During the early stage of the Battersby Township fire, the smoke went straight up in the vertical convection column and thus was mostly injected into the atmosphere above the mixed layer. During the middle stage, the column was occasionally vertical, but mostly it was bent over by stronger winds, and therefore a large fraction of the smoke entered the mixed layer. After the fire ignitions had ceased, the bent-over smoke plume from the smoldering fire had little buoyancy, and the lidar showed a narrow, nearly horizontal smoke plume confined completely in the vertical to the mixed layer. Therefore, all the smoke remained in the mixed layer.

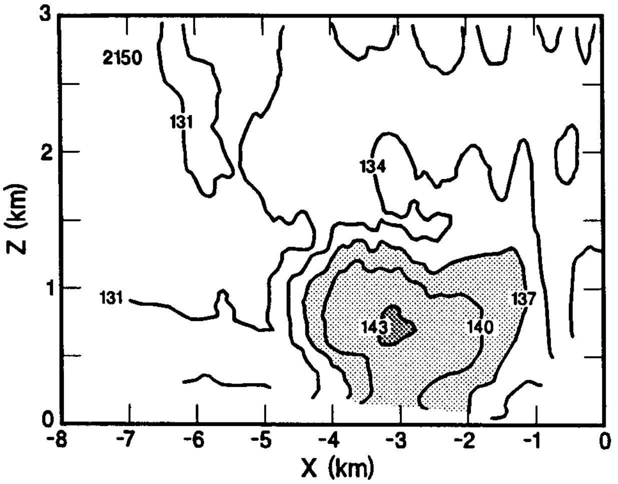

FIG. 14. Vertical cross section of lidar backscatter (dB) through the smoke plume at 2150 UTC. Left in the figure is to the north-northwest along the 340° radial from the lidar (located at $x = 0$). The cross section shows that the main portion of the plume (shaded) passed north-northwest of the lidar and that the strong backscatter was below 1.6 km AGL.

The second question, on the flow structure and kinematics of the convection column, relates to our ability to model and predict the spread and behavior of fires. WPL's Doppler radar mapped the velocity structure of a horizontal plane through a nearly horizontal smoke plume and observed slower flow along the centerline and faster flow along the edges. The Doppler lidar observed one component of the convergent flow below 1.5 km AGL into the convection column. From these analyses we estimated updrafts of 15 m s^{-1} during the first stage of the burn, when the convection column rose nearly straight up to 1.5 km in very light environmental winds, and of 24 and 10 m s^{-1} at two times later in the burn. Because the lidar did not scan down to the base of the fire, these are underestimates, and they do not include the very large turbulent updrafts observed in the combustion zone (Palmer 1981). Lidar data also showed gravity waves during several stages of the fire, and one of the lidar analyses showed strongly descending inflow air upwind of the convection column.

The first of three issues related to convection-column flow structure was the structure of wind-driven fires as opposed to that of buoyancy-dominated fires. Buoyancy-dominated fires, though encountered less often than wind-driven fires, are more unpredictable and often more dangerous. The convection column observed by the radar in Colorado was driven by strong winds. The column observed by the lidar in Ontario was buoyancy dominated up to 1.5 km AGL during the first hour of ignitions, then became increasingly wind driven as the afternoon proceeded. Data in this study thus represented both types of fire.

The second issue in convection-column kinematics was the role of rotation in the intensification of fires. The Doppler radar data signified a pair of counterrotating horizontal vortices for the bent-over convection column of the Left Hand Canyon forest fire, produced by the strong, 13 m s^{-1} ambient flow. The lidar found whole-column rotation in the vertical column, with vorticity estimated at approximately 10^{-2} s^{-1}. This was observed during the early, light-wind stages of the burn. These were examples of type I and type II vortices, respectively, as defined by McRae and Flannigan (1990).

The third issue was the role of models in improving prediction and the role of remote-sensing observations in improving models. The issue for this study is the role of high-quality, high-resolution observations in the improvement of models. It is obvious that empirically based, conceptual models are no better than the observations on which they are based. Numerical model runs similarly require accurate observations for initialization and for verification of results. In the case of column-rotation experiments, for example, observations of the internal kinematics of fire columns, such as those presented this study, would be extremely valuable in validating the model results. Another potentially powerful application of remotely sensed velocity data is using such high-resolution, three-dimensional volumes of data in four-dimensional data-assimilation schemes to provide analyses of both the dynamic and the thermodynamic fields. The velocity observations are used to ensure that the dynamic fields agree with those observed, and the dynamic model provides the unmeasured fields (e.g., pressure and temperature) and assures that these fields are consistent with the governing equations.

We conclude with remarks on the simultaneous use of two lidar–radar systems to improve the quality of the velocity data. The main limitation on the kinematic analyses presented in this study was that they were based on a single instrument, and thus only one wind component, u_r. The cross sections of w presented in this paper were based on the divergence of only u_r. Because winds most likely converge into a fire column from all sides, it is obvious that these cross sections gave underestimates of the actual (total) w. We compensated for this by assuming what are probably reasonable values of w for the other, cross-beam component of the divergence, based on the symmetry of the convection-column system or based on the lidar being almost directly downwind of the fire. The accuracy of estimates of total w relied on the validity of this assumption about the component of the velocity divergence across the lidar beam. In cases where the lidar is not downwind or the flow does not exhibit such symmetry, it will be difficult to have confidence in w analyses and estimates. For these cases it would be best to have two instruments probing the fire (two radars, two lidars, or a lidar and a radar). Having two instruments that can each simultaneously measure u_r inside a fire column allows dual-Doppler estimates of w to be made in and around a fire (Miller and Strauch 1974). By explicitly measuring two components, this technique avoids the need for assumptions about an orthogonal horizontal component of the wind.

Added benefits of using both a lidar and a radar to study a convection column are that data at two wavelengths give more information on particle sizes and shapes, and that the two instruments provide velocity data in complementary regions outside the convection column. The lidar provides data in clear air close to topography, but not in cloud. The radar provides data in cloud but has coarser angular resolution and does not provide data close to topography.

Acknowledgments. The authors gratefully acknowledge Larry Radke of the University of Washington (now of the National Center for Atmospheric Research), who led the effort to take the lidar to Ontario and who has aided our analysis by providing data from Washington's radiosonde and aircraft. This research was funded by the Defense Nuclear Agency via subcontract from the University of Washington. We also had helpful discussions with Brian Stocks, Doug McRae, Chris Grund, Ralph Nelson, and Larry Radke. Darold Ward provided suggestions for issues to be addressed in the Introduction, which we adopted.

We thank Matthew Savoie for his skill in figure preparation and data analysis, and Christine Sweet and Lorraine Kaimal for their technical editing of the manuscript. We also thank Darold Ward, John Cockayne, Chandran Kaimal, Brian Stocks, Doug McRae, Thomas Y. Palmer, and Taneil Uttal for their helpful reviews of the manuscript, and Richard Pelis for providing us with the estimates for the acreage of the Left Hand Canyon fire.

REFERENCES

Aronovitch, B. B., 1989: Forecasting wildfire "blowup." *Proc. 10th Conf. on Fire and Forest Meteorology,* Ottawa, Canada, Society of American Foresters and Amer. Meteor. Soc., 391–399.

Browning, K. A., and R. Wexler, 1968: The determination of kinematic properties of a wind field using Doppler radar. *J. Appl. Meteor.,* **7,** 105–113.

Byram, G. M., 1954: Atmospheric conditions related to blowup fires. Station Paper 35, U.S. Dept. of Agriculture, Forest Service, Southeastern Forest Experiment Station, Asheville, NC. 34 pp.

——, 1959: Forest fire behavior. *Forest Fire: Control and Use,* K. P. Davis, Ed., McGraw-Hill, 90–123.

Church, C. R., J. T. Snow, and J. Dessens, 1980: Intense atmospheric vortices associated with a 1000 MW fire. *Bull. Amer. Meteor. Soc.,* **61,** 682–694.

Cotton, W. R., 1985: Atmospheric convection and nuclear winter. *Amer. Sci.,* **23,** 275–280.

Graham, H. E., 1955: Fire whirlwinds. *Bull. Amer. Meteor. Soc.,* **36,** 99–103.

Haines, D. A., and M. C. Smith, 1987: Three types of horizontal vortices observed in wildland mass and crown fires. *J. Climate Appl. Meteor.,* **26,** 1624–1637.

Hall, F. F., Jr., R. M. Huffaker, R. M. Hardesty, M. E. Jackson, T. R. Lawrence, M. J. Post, R. A. Richter, and B. F. Weber, 1984: Wind measurement accuracy of the NOAA pulsed infrared Doppler lidar. *Appl. Opt.,* **23,** 2503–2506.

——, R. E. Cupp, R. M. Hardesty, T. R. Lawrence, M. J. Post, R. A. Richter, and B. F. Weber, 1987: Six years of pulsed-Doppler lidar field experiments at NOAA/WPL. Preprints, *Sixth Symp. on Meteorological Observations and Instrumentation,* New Orleans, American Meteorological Society, 11–14.

Hardesty, R. M., T. R. Lawrence, R. A. Richter, M. J. Post, F. F. Hall, Jr., and R. M. Huffaker, 1983: Ground-based coherent lidar measurement of tropospheric and stratospheric parameters. *Proc. SPIE,* **415,** 85–91.

——, ——, and R. E. Cupp, 1987: Performance of a 2-J/pulse injection-locked TEA laser for atmospheric wind measurements. *Conf. on Lasers and Electro-optics,* Digest Series, Vol. 14, Baltimore, Optical Society of America.

Hess, S. L., 1959: *Introduction to Theoretical Meteorology.* Holt, Rinehart and Winston, 362 pp.

Hobbs, P. V., and L. F. Radke, 1969: Cloud condensation nuclei from a simulated forest fire. *Science,* **163,** 279–280.

Lhermitte, R. M., 1969: Note on the observation of small-scale atmospheric turbulence by Doppler radar techniques. *Radio Sci.,* **4,** 1242–1246.

Lilly, D. K., 1986: The structure, energetics and propagation of rotating convective storms. Part II: Helicity and storm stabilization. *J. Atmos. Sci.,* **43,** 126–140.

Lyman, H., 1918: Smoke from Minnesota forest fires. *Mon. Wea. Rev.,* **46,** 506–509.

McRae, D. J., and M. D. Flannigan, 1990: Development of large vortices on prescribed fires. *Can. J. For. Res.,* **20,** 1878–1887.

Miller, L. J., and R. G. Strauch, 1974: A dual Doppler radar method for the determination of wind velocities within precipitating weather systems. *Remote Sens. Environ.,* **3,** 219–235.

Mohr, C. G., and L. J. Miller, 1983: CEDRIC—A software package for Cartesian space editing, synthesis, and display of radar fields under interactive control. Preprints, *21st Conf. on Radar Meteorology,* Edmonton, Alberta, Canada, Amer. Meteor. Soc., 569–574.

——, ——, R. L. Vaughn, and H. W. Frank, 1986: Merger of mesoscale data sets into a common Cartesian format for efficient and systematic analysis. *J. Atmos. Oceanic Technol.,* **3,** 143–161.

Molencamp, C. R., and M. M. Bradley, 1991: Numerical simulation of the dynamics and microphysics of prescribed forest burns. *Proc. 11th Conf. on Fire and Forest Meteorology,* Missoula, Montana, Society of American Foresters and Amer. Meteor. Soc., 447–454.

Moninger, W. R., and R. A. Kropfli, 1987: A technique to measure entrainment in cloud by dual-polarization radar and chaff. *J. Atmos. Oceanic Technol.,* **4,** 75–83.

Palmer, T. Y., 1981: Large fire winds, gases and smoke. *Atmos. Environ.,* **15,** 2079–2090.

——, and L. I. Northcutt, 1972: A high temperature water-cooled anemometer. *Fire Technol.,* **7,** 201–204.

——, T. C. Goodale, and S. B. Martin, 1991: Layer replacement in wildland fire. *Proc. 11th Conf. on Fire and Forest Meteorology,* Missoula, Montana, Society of American Foresters and Amer. Meteor. Soc., 593–597.

Penner, J. E., L. C. Haselman, Jr., and L. L. Edwards, 1986: Smoke-plume distributions above large-scale fires: Implications for simulations of "nuclear winter." *J. Climate Appl. Meteor.,* **25,** 1434–1444.

Pittock, A. B., T. P. Ackerman, P. J. Crutzen, M. C. MacCracken, C. S. Shapiro, and R. P. Turco, 1986: *Environmental Consequences of Nuclear War, Volume I: Physical and Atmospheric Effects.* John Wiley & Sons, 359 pp.

Post, M. J., 1978: Experimental measurements of atmospheric aerosol inhomogeneities. *Opt. Lett.,* **2,** 166–168.

——, and R. E. Cupp, 1990: Optimizing a pulsed Doppler lidar. *Appl. Opt.,* **29,** 4145–4158.

——, R. A. Richter, R. M. Hardesty, T. R. Lawrence, and F. F. Hall, Jr., 1981: NOAA's pulsed, coherent, infrared, Doppler lidar—Characteristics and data. *Proc. SPIE,* **300,** 60–65.

Radke, L. F., and J. D. Locatelli, 1988: Radiosonde data for Battersby and Peterlong prescribed fires, Ontario, Canada, August 1988. University of Washington, Department of Atmospheric Science, 28 pp.

——, and P. V. Hobbs, 1991: Humidity and particle field measurements around some small cumulus clouds. *J. Atmos. Sci.,* **48,** 1190–1193.

——, and D. E. Ward, 1991: Prescriptions for biomass fire smoke reductions. *Proc. 11th Conf. on Fire and Forest Meteorology,* Missoula, Montana, Society of American Foresters and Amer. Meteor. Soc., 460–469.

——, D. A. Hegg, P. V. Hobbs, J. D. Nance, J. H. Lyons, K. K. Laursen, R. E. Weiss, P. J. Riggan, and D. E. Ward, 1991: Particulate and trace gas emissions from large biomass fires in North America. *Proc. of the Chapman Conference on Global Biomass Burning: Atmospheric, Climate, and Biospheric Implications,* MIT Press, 569 pp.

Rothermel, R. C., 1991: Predicting behavior and size of crown fires in the northern Rocky Mountains. Res. Pap. INT-438. U.S. Dept. of Agriculture, Forest Service, Intermountain Research Station, Ogden UT. 46 pp. [Available from Intermountain Research Station, 324 25th St., Ogden UT 84401.]

Shostakovitch, V. B., 1925: Forest conflagrations in Siberia. *J. Forestry,* **23,** 365–271.

Smith, C. D., Jr., 1950: The widespread smoke layer from Canadian forest fires during late September 1950. *Mon. Wea. Rev.,* **78,** 180–184.

Wexler, H., 1950: The great smoke pall—September 24–30, 1950. *Weatherwise,* **3,** 129–142.